CRANFIELD UNIVERSITY

C. SEYNAT

QUANTIFICATION OF THE EFFECT OF WIND DRIVEN WHEAT MOTION ON SAR INTERFEROMETRIC COHERENCE

COLLEGE OF AERONAUTICS

PhD THESIS

CRANFIELD UNIVERSITY

COLLEGE OF AERONAUTICS

PhD THESIS

Academic Years 1997-2000

C. SEYNAT

Quantification of the effect of wind driven wheat motion on SAR interferometric coherence

Supervisor: Dr S.E. Hobbs

October 2000

This thesis is submitted in partial fulfilment of the requirements for the degree of Doctor of Philosophy

Abstract

This report quantifies the motion of wheat subject to wind and assesses the effect of this motion on the coherence obtained from Synthetic Aperture Radar (SAR) interferometry. Over vegetation, the loss of coherence due to the change in backscatter between two SAR images taken at a different time (temporal decorrelation) is related to the wind induced motion of vegetation elements. The research aims to provide simultaneous *in situ* measurements of crop motion and wind velocity at canopy height and to use these measurements in a coherence model to determine the quantitatively the parameters which infer temporal decorrelation. The potential of coherence for agricultural applications is assessed.

The three-dimensional motion of wheat is measured by a photogrammetry method using two commercially available video cameras. Simultaneously, wind velocity at canopy height is measured by anemometers at a high sampling frequency. Wheat motion and wind velocity data were collected in a field local to Cranfield University in summer 2000. The CD attached to this report contains the wheat motion and wind velocity data. They show that the motion of wheat is correlated with the wind speed, and that wheat plants adjacent to each other move coherently.

The coherence model is based on a statistical approach, which represents the total backscatter from vegetation as the phasor addition of a fixed component and one or more components which are weather dependent. The relative contributions of the total backscatter are estimated with the RT2 backscatter intensity model. The motion measurements are used to define the variability of the phase of the weather dependent components in the model.

Outputs of the model show that a C-band SAR with an incidence angle of 23° (typical configuration of the ERS satellites) yields coherence values highly variable with the wind conditions at the time of the radar passes. The potential use of coherence for agricultural applications is limited by this variability, which infers the need for an accurate coherent backscatter model.

Acknowledgements

Je tiens à ce que les seuls mots en français de cette thèse soient les premiers, afin d'exprimer ma gratitude à mes parents, Jocelyne et Jean-Paul, pour leur soutien pendant mes longues années d'études de Saintes à Cranfield.

I wish to thank my supervisor, Dr Hobbs, for his help during the production of this thesis, for sharing his experience with me during a number of interesting discussions, and for the very valuable learning experience I gained from him. I also appreciate the cooperation of the College of Aeronautics staff who provided me with the equipment and advice I requested from them, Dr Oswald and Ramesh Wadher in particular. Thanks are also due to Mr Hobbs for letting me invade his wheat field on several occasions. GEC-Marconi has provided a copy of the RT2 model used in this research, and the ERS SAR data was given by the European Space Agency.

Three years of research would not be possible without the moral support of friends. I cannot name them all here, but I gratefully thank them for making of this experience in the UK an episode of my life which I will remember for many years to come.

I wish to direct the final thoughts of these acknowledgements to Ilse, for the moral support she constantly provided, even with the long distance which separated us.

Contents

List of Figures

List of Acronyms

ACF	Autocorrelation Function
ADC	Analogue to Digital Converter
AOI	Area Of Interest
AVI	Audio Video Interleave
AWS	Automatic Weather Station
CCF	Cross-correlation Function
DAC	Digital to Analogue Converter
DEM	Digital Elevation Model
DV	Digital Video
DVA	Digital Vane Anemometer
FFT	Fast Fourier Transform
GMT	Greenwich Mean Time
IDL	Interactive Data Language
InSAR	SAR Interferometry
LAI	Leaf Area Index
LED	Light Emitting Diode
LM	Levenburg-Marquadt
MIMICS	Michigan Microwave Canopy Scattering
PRI	Precision Image
PRF	Pulse Repetition Frequency
RMS	Root Mean Square
SAR	Synthetic Aperture Radar
SIR	Shuttle Imaging Radar
SLC	Single Look Complex
SNR	Signal-to-Noise Ratio
SVD	Singular Value Decomposition

Chapter 1

Introduction

This report presents research undertaken at Cranfield University from October 1997 to October 2000. The origins of the study lie in the remote sensing of crops for agricultural applications. Airborne or spaceborne sensors can provide information about a wide range of properties of the Earth's surface and can serve a variety of purposes, from the determination of the geographical extent of man-made features to the retrieval of geophysical or biophysical parameters. Agriculture is an application where these two purposes are well illustrated: remote sensing can provide geographical information about agricultural fields on a global scale, and can also be used to retrieve quantitative information about relevant parameters such as crop yield.

Traditionally, the remote sensing of agricultural fields is performed mainly in the optical domain, and commercial applications nowadays use data collected in the visible and near infrared parts of the electromagnetic spectrum. Optical data sources are used to give crop statistics and make yield forecasts on a global scale, and contribute to define policies for agricultural planning and monitoring at a national or European level. Health indexes can also be derived from optical data.

With the advent of radar remote sensing satellites, a new source of potential information arose, opening the possibility to access novel or more accurate knowledge about the properties of the Earth's surface. In addition to this, microwaves have the capability to penetrate clouds and to be used regardless of the sun's illumination, including at night. Therefore, radar remote sensing is in principle more adapted to provide a continuous coverage of the globe. For these reasons, the use of Synthetic Aperture Radar (SAR) and of SAR interferometry (InSAR) for agricultural applications has received increasing attention in the past decade. In SAR interferometry, the complex degree of coherence is a quantitative indicator of the correlation between two SAR images of the same area. Among other effects, the coherence is influenced by the temporal changes which affect the Earth's surface between the time of the two images. On short time scales, the main time dependent source of reduction of the coherence magnitude ("decorrelation") from SAR data above vegetated areas is related to the motion of the plants or trees subject to wind. Behind this relation between the coherence and vegetation lies a potential source of information about crops, and the justification for the work presented in this report.

Only very recent published studies have tried to relate the coherence from SAR

data to parameters representative of the properties of crops or forest. They have in common that they identify as a key missing element the observations of plant response to wind, from which models could be used to quantify decorrelation mechanisms and consequently determine the amount of information carried by the coherence about crops. Making an accurate quantitative estimate of the way crops move in the wind is *a priori* rather difficult because of the random nature of the motion. Other difficulties include the variability of this motion under different wind conditions and the fact that a measurement system should be entirely non-invasive so it does not impinge on the natural movements of the crops.

Aim and objectives of the research

It is the aim of the project to make a useful contribution concerning the issues raised above. Cranfield University had built valuable experience in the fields of radar remote sensing and micrometeorological research, and the two aspects can be combined for the purpose of the study presented here. The first objective of the project is to develop a methodology to measure the motion of crops in different wind conditions. The second objective is to use the measurement system to provide a database of motion observations, in parallel with wind velocity measurements at canopy level, and to analyse the relation between the two. The third objective is then to show how the knowledge acquired from the measurements can be used to estimate the coherence to expect from agricultural fields, and to state on its potential use for operational applications.

Methodology

The project uses digital photogrammetry to retrieve the position of crop elements in three dimensions. Consumer digital video cameras are used in a wheat field for *in situ* measurements, together with anemometers suitable for micrometeorological applications. Since the objective of the research is to demonstrate the methodology to make accurate measurements, the study focuses on wheat, which is a geometrically simple plant. However, the methodology can be applied to other crops. The measurement system is used in a wheat field local to Cranfield University, in the summer 2000. The output of the measurement campaign is a series of wind velocity and wheat motion data files. From them, a simplified (statistical) estimator of the coherence is developed and used to provide information about the parameters affecting the coherence and to evaluate its potential for agricultural applications.

Structure of the report

The introductory lines above outline the project as a whole, but it is clear that it requires a more precise justification and definition of its objectives and expected outputs. Chapter 2 provides a background to radar remote sensing, SAR interferometry and the use of coherence for vegetated areas, which can be used to clarify the scope of this research. Once the project is placed in its context, its objectives and outputs are detailed. Chapter 3 uses a radar backscatter model to present the parameters affecting primarily the backscatter intensity from crops. It then moves

on to show the basis of the coherence estimator which will use the measurements of wheat motion. The output of Chapter 3 is a list of specifications which drive the design of the crop motion measurement system. The three-dimensional motion measurement system and the anemometry package are described in Chapters 4 and 5 respectively. The use of digital video cameras widely available constitutes an original part of the research, in that it shows how scientific use can be made of commercially available technology, therefore combining accuracy and reduced development cost. Chapter 6 describes the wheat motion and wind velocity data sets collected during summer 2000, and presents an analysis of the relation between the two. From this analysis, Chapter 7 uses the coherence model introduced in Chapter 3 to show the influence of the radar configuration and of the wind conditions on the coherence. The analysis highlights some of the potential uses and limitations of the coherence for crop monitoring.

The wheat motion and wind velocity measurement method, the creation of a database of measurements in the summer 2000, and insights into the capacity of the coherence to be used for crop monitoring, are the key issues this report addresses, in the hope that readers will find them useful for their personal research and interests.

Chapter 2

Background and objectives

Before presenting the objectives of the research it is important to be aware of some of the major milestones which have led to the current state of the art in the field of radar remote sensing. For this reason a historical perspective is required and will be briefly presented in the next section. It includes a brief history of radar systems and of Synthetic Aperture Radars (SAR), before moving on to describe the past and current uses of SAR platforms for Earth Observation, with a final emphasis on agricultural monitoring. Through this description of the past and current techniques of SAR remote sensing, including the more recent use of interferometry, the issues this thesis deals with will become more clear. The concluding lines of Section 2.1 identify a more precise area for the research.

Clear objectives and outputs of the thesis cannot be defined without discussing some necessary theoretical principles. These are the subject of Section 2.2, which presents the principles of SAR image formation and their associated properties, of SAR interferometry and of the complex degree of coherence. Then the current use and the limitations of SAR interferometric (InSAR) coherence in vegetation remote sensing applications are presented (Section 2.3). For reasons detailed in Section 2.3, one of the limiting factors in our understanding and use of the coherence for vegetation monitoring is linked to the current lack of measurements of the motion of this vegetation. Section 2.4 presents the state of the art for the measurement of wind-induced vegetation swaying. In response to the limitations put forward both in Sections 2.3 and 2.4, the objectives of the thesis and the methodology used to meet these objectives are finally presented in Section 2.5. The expected outputs of the research are also stated.

2.1 Background and rationale of the research

The roots of this research lie in satellite radar remote sensing, and it is important here to give a general background on this technique, in particular for vegetation monitoring purposes. The aim of this section is to provide an overview on the past, current, and future developments of SAR remote sensing. Details relating more precisely to the remote sensing of vegetation with SAR interferometry will be given in Section 2.3.

2.1.1 A brief history of radar systems and spaceborne SAR missions

A chronological overview of the evolution of radar systems used for imaging purposes is presented in [2]. Basically, a radar is sends pulses of electromagnetic energy in the microwave region of the electromagnetic spectrum, and receiving part of this energy after reflection by any physical object subjected to the radiation. The first steps towards the practical use of radar systems were made between the initial works of the German scientist Hertz at the end of the 19^{th} century and the beginning of the Second World War. In that period, ground-based radars were used for the detection and tracking of ships and aircraft. The first airborne radars were developed during the Second World War for military purposes.

The first operational Synthetic Aperture Radar systems were developed at the beginning of the 1950's, but it is only in the 1960's, with the declassification of the SAR technique, that civilian applications were started, for geology, land-use, and vegetation studies. A wealth of independent developments kicked off in the 1970's, with the use of digital image processing techniques.

The first spaceborne SAR system was on the Apollo-17 spacecraft in 1972 for geological and topographic mapping [3]. The radar interferometry technique for surface mapping of Venus was used in 1978 on board Pioneer-12. The first Earth imaging civilian SAR antenna was on NASA's SEASAT in 1978, and is a milestone in spaceborne radar remote sensing. Not only was the SEASAT SAR an excellent technology demonstrator, but it is also the source of many publications for a wide variety of applications. In the 1980's, the Shuttle Imaging Radar (SIR) series started and still carries on nowadays on Space Shuttle missions. The SIR missions often broke new ground in SAR technology, from the first mechanically steerable antennas for use at a variety of incidence angles, to the current use of SIR-C/X which offers a variety of wavelengths, incidence angles, polarisations, and resolutions.

The 1990's mark the arrival of newcomers on the spaceborne SAR market. In 1991, the European Space Agency launched ERS-1, carrying a SAR antenna among other scientific payloads. It was followed by ERS-2 in 1995, a copy of ERS-1. The Japanese JERS-1 was launched in 1992, and the Canadian RADARSAT in 1995, both with a SAR system on board.

The radar interferometry technique was tested on Venus and on the Moon from Earth-based antennas for topographic purposes in 1971-1974. SAR interferometry was demonstrated from an airborne platform in 1974 [4] and from space at the end of the 1980's [5]. But the major advances in SAR interferometry originate from the data collected by the ERS-1/2 satellites after 1995, and is still a vivid source for today's research. The Shuttle Radar Topographic Mission (SRTM) is currently the most recent database of interferometric data. The data were collected in February 2000 and is being processed.

Future SAR missions are currently under development or are now approaching their launch date. Among these, some of the most awaited for are the ENVISAT Advanced SAR (ASAR), which will provide high resolution SAR data in a wide range of operating modes, incidence angles and polarisations. The RADARSAT-2 satellite, to be launched in 2003, will provide SAR data of a similar standard to that of

ENVISAT. Other interesting developments include the LightSAR concept, a space-borne platform of reduced size and mass, opening the potential use of constellations of SAR satellites for near-continuous Earth observation [6].

2.1.2 Applications of SAR and InSAR for Earth observation

The previous section focused on the past and current SAR missions, and this section now presents the applications of SAR data for Earth observation. In parallel with the radar observations, there has been and there still is a continuous effort to provide the fundamental link between the physical properties of the elements which scatter the incoming radar waves and the radar backscatter signal received by the antenna. This is the modelling approach, which aims to predict the radar backscatter from a given surface (the "direct" problem). From these models, and also from purely empirical observations, the end goal of radar remote sensing can be sought for, i.e. the prediction of the geophysical and biophysical properties of a terrain from radar observations (the "inverse" problem).

Although the direct problem is the subject of constant efforts in the past 15 years in terms of publications [7], the inverse problem is still a fairly new area. The reason for that lies in the fact that most remote sensing missions are now driven by commercial objectives. It is likely that national and international organisations will not fund remote sensing satellites in the future for the unique use of the research community. These organisations now seek to see a return of their investments of the past decades through the development of commercially viable Earth observation applications which can be managed by private funding. Such a situation could be met in the coming years, with the most recent advances in space technology and with the current efforts to improve our understanding of SAR backscattering mechanisms for use in operational applications.

In this commercial context, the current operational applications of SAR data are still limited. Applications such as high resolution, high precision Digital Elevation Models (DEM), disaster monitoring (earthquake, landslides, floods), polar ice motion monitoring, are presently the most advanced. Other potential applications include the monitoring of forests, agriculture, coastal areas, deserts, volcanoes, and land-use classification. Rather than quoting here a series of examples, and in order to get a more clear picture of the current state of SAR research and applications, Figure 2.1 shows the percentage of papers, classified by theme, presented at two recent SAR conferences. These are the Second International Workshop on *Retrieval of Bio- and Geo-Physical parameters from SAR data for land applications*, held at ESA-ESTEC in October 1998, and the *Fringe'99* workshop on SAR interferometry, held in Liège, Belgium, in October 1999.

Although they are based in Europe, these two conferences are international events and are supposed to be a good representation of the current state of the SAR/InSAR research. The first element to note is that SAR interferometry represent approximately 20 % of the current applications. Figure 2.1 shows that agriculture and forestry are applications based on the SAR backscatter intensity, whereas SAR interferometry shows its value mainly in DEM generation, land motion, ice monitoring and volcanology. The two fields, SAR and SAR interferometry, seem to

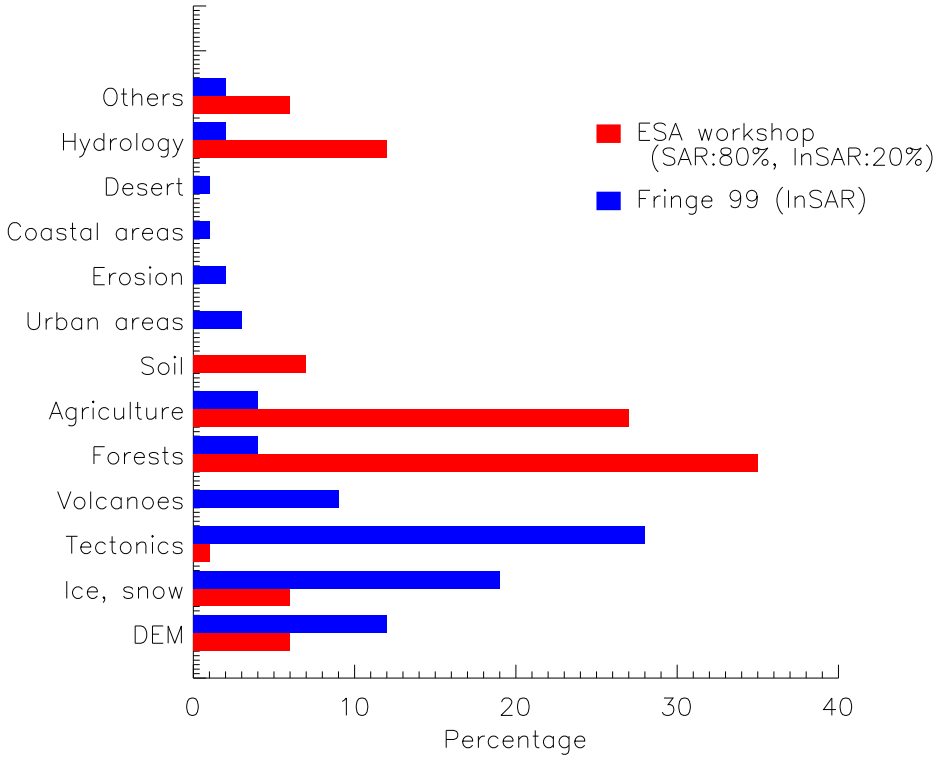

Figure 2.1: Percentage of papers by theme at two recent SAR/InSAR conferences

be fairly well delimited in terms of these applications and are complementary rather than competing against each other.

The two major types of vegetation on land are forest and agricultural crops. The assessment of vegetation characteristics aims to get quantitative estimates of variables such as productivity, crop yield, or mass and energy budgets of soil and vegetation. These parameters are important for two major reasons. First they will enhance our current understanding of the processes underlying environmental change. Global hydrological models and carbon cycle models heavily depend on an estimate of some key vegetation parameters which can in principle be accessed on a global scale by spaceborne remote sensing techniques. The second aspect, more focused on the commercial side, is that assessing agricultural crop characteristics can help agricultural planning and policy at a national or European level. SAR and InSAR data currently find more uses in forestry applications [8, 9, 10] than for agriculture, although the potential of the latter is acknowledged [11]. Agriculture monitoring from SAR data is therefore still at the research level. It is stated in [12] that a wide range of agricultural crops (wheat, barley, rice, etc...) have been the subject of recent research with the use of SAR data. One particularly important aspect of these studies is that they use multi-temporal data for improved accuracy, in particular to discriminate between different crop types. New techniques are developed to classify crops from SAR data, a number of which make use of optical data as a valuable complement.

The use of SAR interferometry and in particular of the coherence for agriculture monitoring is still very marginal, although it is pointed out in [12] as an area to

investigate in the future. Most studies focus on the retrieval of crop height from InSAR data [13, 14, 15], based on empirical relations derived from field observations. Details on these techniques will be given in section 2.3.

2.1.3 Complementarity SAR/Optical for vegetation monitoring

A wide range of sensors can be used in space, covering different windows in the electromagnetic spectrum. Each spectral domain is sensitive to one or more characteristics of a particular canopy and soil. The optical domain will provide estimates of canopy variables such as the leaf area index and of the biochemical composition. The thermal infrared domain and passive microwave will show some sensitivity to surface temperature and canopy structure. The active microwave domain is used to obtain information on soil roughness, moisture, canopy structure. The use of combined data from different sources is potentially very valuable to get a wide range of information on the canopy.

Complementarity between ERS SAR interferometry data and optical data from the SPOT satellite is demonstrated in [16] and marketed by the company SPOT-Image: the mapping of deforestation in the rainforest is possible with a combined SAR/Optical data set. In the more specific case of agriculture, the use of optical data for crop classification has been demonstrated, and some health indexes can also be derived from it. However, optical data can only be used in good weather (cloud-free) conditions, which is one of its major limitations. In particular, for countries almost always covered by clouds at least partially, getting consistent time series for multi-temporal analysis is virtually impossible.

It is mainly for this reason that the use of SAR data for agriculture applications is being investigated. Its potential should at least be assessed before it can be rejected. The current opinion in the remote sensing community is that SAR interferometry does not have the potential to provide on its own better results than optical data, but there is certainly the possibility that it can provide some information about the vegetation cover, which is more than optical satellites can give on cloud-covered surfaces. In addition to this, since optical data and SAR data show sensitivities to different vegetation parameters, there is a potential complementarity between the two.

2.1.4 Rationale for the thesis

Based on the very general introductory overview of the previous sections, it is important to make some preliminary points which have driven the research presented here. Because of his imaging capabilities in all weather conditions, day and night, it was first thought that SAR data would be the panacea for most remote sensing issues. Today, views on this point have changed in the SAR community. There is very little doubt that SAR data provides information about a wide range of properties of the Earth cover, but the extent and the quantitative usefulness of this information was probably misjudged. Fifty years after the creation of the first operational SAR, and despite the impressive improvement in SAR technology, scientists are still

struggling to find commercially viable applications worthy of the initial interest SAR had generated. The need to find these applications is the major concern of today's remote sensing conferences. Operational readiness and marketing of SAR products are at the centre of attention more than ever before, mostly because international and national organisations will not indefinitely fund a research area which cannot prove its commercial viability.

For this reason, the current trend in SAR remote sensing is to push towards the development of these commercial applications, but this is sometimes done at the expense of our understanding of the underlying physics which govern the SAR backscattering mechanisms. There is now a lot of work being put into the development of commercial SAR applications based on physical properties which are still difficult to model and to understand. Fortunately scientists have not forgotten that the need to understand what sensors truly measure is the key to the development of a future market [7].

The work presented here is written with these two aspects constantly in mind. This research is driven by the need to understand the physical mechanisms affecting SAR and InSAR data, not for a simple intellectual satisfaction, but to provide useful information about the potential of SAR interferometry for agricultural applications.

It was shown in the previous sections that very little work has been published to relate InSAR data and crop parameters. This is probably due to the fact that optical data and SAR intensity data are already well established sources of information that can be used for crop monitoring. The use of InSAR coherence for agricultural applications is therefore a rather novel area of research and is interesting at least in that respect. But the relation between coherence and crop parameters should be studied mainly because it would otherwise be neglecting a potential source of valuable information. The following sections will highlight this potential, which is the basis of the research objectives stated in section 2.5.

2.2 Introduction to SAR theoretical principles

It is not possible to define precise objectives for the research without giving some background theory on radar backscatter, SAR, and SAR interferometry. The following sections fill this gap. The issues of radar backscatter and SAR interferometry have been the subject of far too much research to be reproduced here in their entirety. However, it is relevant to introduce the concepts which will be used in the remainder of this report, in particular those relevant to the remote sensing of crops.

2.2.1 Radar backscatter: definition of relevant parameters

The microwave spectrum is the part of the radio spectrum which extends throughout the Ultra, Super and Extremely High Frequency bands (UHF, SHF, EHF, respectively), from about 0.3 GHz to about 300 GHz in frequency (1m to 1mm in wavelength). The microwave spectrum is divided into several bands designated by the letters summarised in Figure 2.2 [17].

All radar remote sensing studies deal with the parameter σ^0, originally defined as the differential (back)scattering coefficient, but mostly referred to simply as the

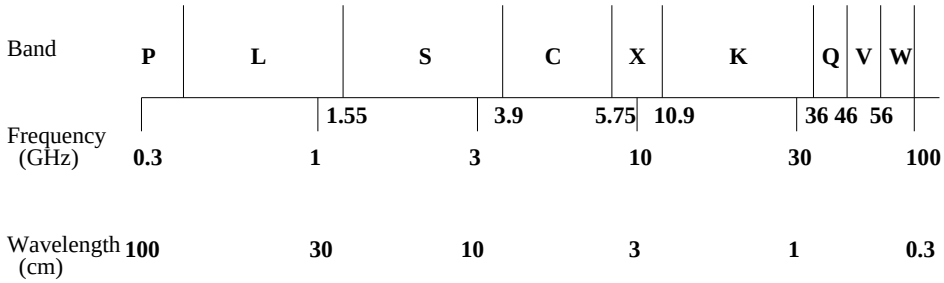

Figure 2.2: The microwave spectrum

(back)scattering coefficient. The prefix `back´ is used in the monostatic case, i.e. when there is only one radar antenna used as a transmitter and receiver of the radar signal, which is the case of active microwave remote sensing . A brief definition of σ^0 is required here, and it originates in the radar equation [18]. An antenna of area A (m^2) transmits an electromagnetic wave of wavelength λ (m), radiating a total transmitted power P_t (W) in a pattern mainly dependent on the antenna geometry. A target at a distance R (m) is hit by this incoming wave and reflects a part of it back to the antenna. The part of the incoming signal which is reflected back to the antenna depends on the size of the target, its absorbing and reflective properties in the direction of the antenna. These properties are regrouped in a single parameter, σ, the scattering cross-section. It is shown for example in [18] that the power P_r (W) received back at the antenna can be written:

$$P_r = \frac{P_t A^2 \sigma}{4\pi\lambda^2 R^4} \tag{2.1}$$

In reality, there is not a single scatterer in the scene observed but several targets, each of which can have a different scattering cross-section σ_i. For this reason, it is necessary to introduce an average scattering cross-section. The differential scattering coefficient is introduced for this purpose, and is defined as:

$$\sigma^0 = \langle \frac{\sigma_i}{\Delta A_i} \rangle \tag{2.2}$$

Here ΔA_i represents an area on the ground over which the parameters of Equation (2.1) remain nearly constant. In remote sensing applications the differential backscattering coefficient is called the backscattering coefficient. It is a dimensionless number, usually expressed in Decibels (dB):

$$\sigma^0(dB) = 10 \ln \sigma^0 \tag{2.3}$$

The polarisation [17] of the incoming wave also influences the values of σ^0. Most remote sensing applications only deal with vertically and horizontally polarised waves, so that it is common to define four different backscattering coefficients $\sigma^0_{VV}, \sigma^0_{HH}, \sigma^0_{VH}, \sigma^0_{HV}$, where the first letter represents the polarisation of the incoming wave and the second letter that of the outgoing wave. Polarisation can be an important aspect when considering the backscattering from a vegetation medium.

The parameters of the scattering medium which influence the value of σ^0 are numerous and the subject of modelling studies for the past 30 years. In the case of

surface scattering, the two main parameters to affect σ^0 are the surface roughness (root mean square height relative to a smooth surface) and the dielectric constant ε. If the surface roughness is small compared to the radar wavelength, the scattering mechanism is near specular and σ^0 takes low values. It should also be noted that a portion of the incoming energy will also be refracted at an angle function of ε, itself dependent on soil moisture. Other scattering mechanisms will occur as the surface roughness increases with respect to the wavelength. A thorough description of surface scattering modelling can be found in [18].

Most natural surfaces are penetrated by the incoming radar wave, at least partially and for certain wavelengths. Consequently the scattering occurs mostly within a volume rather than on a surface. The properties of the scattering volume determine the backscatter coefficient, and the modelling of the volume scattering mechanisms is usually specific to the type of volume considered. The two main approaches to model volume scattering are based on wave theory and radiative transfer theory. Wave theory is based on Maxwell's equations of electromagnetism and accounts for the coherent addition of waves travelling in different directions in the scattering volume. Radiative transfer theory considers the transport of energy in the volume. The wave theory is usually more difficult to use as it needs a very precise definition of the configuration of the scattering volume but the radiative transfer theory cannot account for wave effects and can therefore lead to erroneous estimates of the backscatter in some cases.

2.2.2 Principles of SAR image formation

SAR geometry and system parameters

The creation of SAR images requires complex signal processing which is described in detail in many textbooks [19]. Only the relevant principles are given here. The typical geometry for SAR measurements is presented in Figure 2.3. A radar antenna of length l and width w is carried on a platform (airborne or spaceborne) at a velocity V and altitude h. The antenna is looking sideways at an angle θ, and repeatedly radiates radio pulses of duration τ_p at a rate defined by the Pulse Repetition Frequency (PRF). The transmitted pulse has a carrier frequency f_0, corresponding to a wavelength $\lambda = c/f_0$, where c is the speed of light. Antenna theory shows that the radiation transmitted by an antenna of length l spans over an angle λ/l. $\theta_a = \lambda/l$ on Figure 2.3 is the angle over which each pulse is radiated in the azimuth direction (denoted by the x coordinate). R being called the range, i.e. the distance from the radar to the surface, the similar angle in the range direction is $\theta_R = \lambda/w$.

The geometry presented here is simplified, as it does not take into account additional parameters related to the Earth's curvature. The `flat Earth´ case is sufficient to understand the principles of SAR image formation.

Processing a single pulse - The range dimension

The transmitted pulse of duration τ_p extends spatially over a distance $c\tau_p$. The projection of this spatial extent on the surface defines the achievable ground resolution

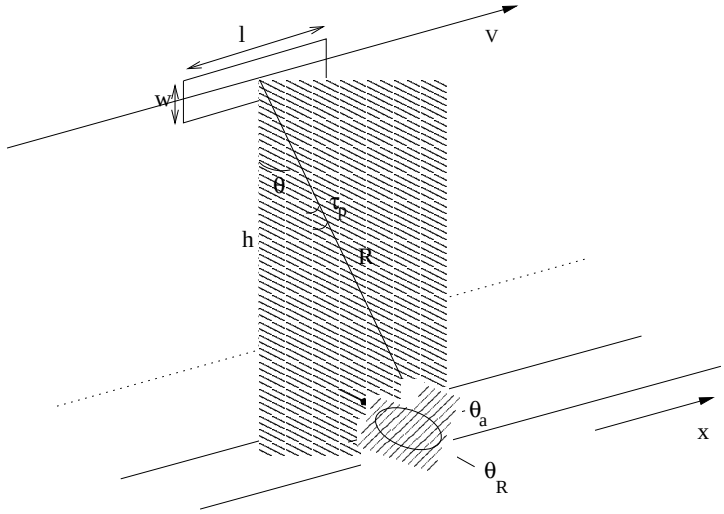

Figure 2.3: SAR geometry and system parameters

r_g for the radar system:

$$r_g = \frac{c\tau_p}{2\sin\theta} \tag{2.4}$$

where the factor 2 accounts for the two-way propagation of the pulse.

With the ERS parameters, where τ_p=37.1 s and $\theta \approx 23°$, the ground resolution would be of the order of kilometers (r_g=14.2 km), which is far from the announced resolution of the order of tens of metres and impractical for most applications. High spatial resolution is achieved by a pulse compression technique. The pulse received at the radar is correlated to a copy of the transmitted signal. This is known in communication theory as matched filtering.

Assuming that the transmitted signal is s(t), an isolated point target produces a response proportional to s(t-τ), where $\tau = 2R/c$ is the delay since transmission. Ignoring for the moment issues related to the amplitude of the signals, the output of the matched filter is:

$$f(t) = \int_{-\infty}^{+\infty} s^*(t'-t)s(t'-\tau)dt' \tag{2.5}$$

where the superscript * denotes the complex conjugate. If the transmitted pulse s(t) is chosen to have a constant spectrum magnitude over a bandwidth B (i.e. $|f - f0| < B/2$), the integration defined in Equation (2.5) shows that the output of the matched filter has a power function $|f(t)|^2$ of the form:

$$|f(t)|^2 = B^2 \left| \frac{\sin\left[\pi B\left(t - 2R/c\right)\right]}{\pi B\left(t - 2R/c\right)} \right|^2 \tag{2.6}$$

$|f(t)|^2$ peaks at t=2R/c, which gives the range of the target. The width of the main lobe is $\delta t \approx 1/B$ and defines the time resolution of the system. The associated ground resolution is $r_g = c\delta t/2\sin\theta$. For ERS, the range bandwidth is B=15.55 MHz, which corresponds to $r_g \approx 25m$ (and a compressed pulse length t=64 ns).

Without pulse compression, the pulse duration required to obtain a high resolution would be very short and the resulting energy per pulse would be too low for

reliable detection. The pulse compression technique therefore allows to have a high resolution and a high signal-to-noise ratio (with a longer transmitted pulse).

Some aspects of the single pulse processing have not been mentioned in the above description. First, the correlation operation is not performed with an exact replica of the transmitted pulse but a weighting function is also present, which results in a reduction of the unwanted secondary sidelobes in f(t), made at the expense of range resolution. The second important aspect not mentioned previously is that the processing is digital, i.e. the compressed signal is sampled. A description of digital SAR processing can be found in [20].

Azimuth processing

The azimuth processing in a SAR system makes use of the phase information contained in the returned signal. More precisely, it uses the variation of the phase of the returned pulses from a single target while this target remains in the ground footprint of the beam.

In order to understand how azimuth processing is achieved, it is useful to introduce some simple notation as shown in Figure 2.4, which is a top view of Figure 2.3. The letter s denotes the time at which a particular target T is viewed by the beam. A convention would for example be to set $s = 0$ when the target T enters the footprint defined by the radar beam, and $s = S$ when the target leaves the footprint. The time here is noted s to refer to 'slow' time, as opposed to the travelling time t of the pulses introduced previously. C is the centre point of the beam. R(s) is the range of the target at time s, and R_c the range of point C. The corresponding azimuths are X(s) and X_c.

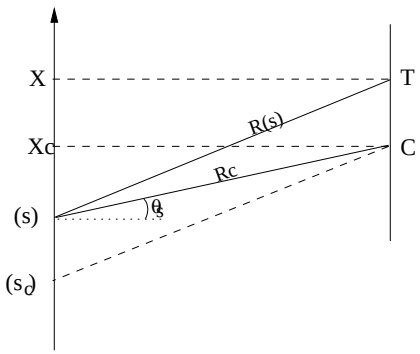

Figure 2.4: SAR geometry for azimuth processing

It can be shown by calculating the integral of Equation (2.5) that the output of the matched filter after demodulation (i.e. removal of the carrier frequency f_0) is of the form:

$$f(t) = exp\left(-\frac{j4\pi R}{\lambda}\right)\frac{\sin x}{x} \tag{2.7}$$

This equation shows the phase term which did not appear in Equation (2.6), where only $|f(t)|^2$ was considered. The term πBt is replaced here by the generic variable x (dependent on the fast time t) to account for the possibility of other treatments on the signal, such as the inclusion of a weighting function mentioned

in the previous section. The actual expression for x is not relevant here anyway, as the azimuth processing uses the phase term $\exp(-j4\pi R/\lambda)$.

The value of f(t) kept for azimuth processing is the peak value with respect to t, i.e. the complex value $exp(-j4\pi R/\lambda)$. For a given target, this value varies with varying range as the radar platform moves. It is therefore a function g of slow time s:

$$g(s) = exp\left(-\frac{j4\pi R(s)}{\lambda}\right) \tag{2.8}$$

Using the geometry of Figure (2.4), the range R(s) can be approximated by:

$$R(s) \approx R_c + \frac{1}{2}V_s^2\frac{(s-s_c)^2}{R_c} + V_s(s-s_c)\sin\theta_s \tag{2.9}$$

Equation (2.9) shows that the phase $\phi = -4\pi R(s)/\lambda$ of g(s) is a function of time, and therefore yields a Doppler effect. The Doppler frequency is defined as $f_D = (1/2\pi)d\phi/ds$ and the Doppler frequency rate is $f_R = (1/2\phi).d^2\phi/ds^2$. By differentiating ϕ with respect to s, the following expression is found for the Doppler frequency rate f_R:

$$f_R = -\frac{2}{\lambda}\frac{V_S^2}{R_C} \tag{2.10}$$

Similarly to range compression, the signal g(s) is correlated to a correlator function. Details on how the correlator function is chosen is not be presented here (see [19] for details), but the output $h(s)$ of the azimuth correlation operation can be shown to be of the form:

$$h(s) = S\frac{\sin\left[\pi f_R S\left(s-s_c\right)\right]}{\left[\pi f_R S\left(s-s_c\right)\right]} \tag{2.11}$$

h(s) peaks for s=s_c, which gives the target azimuth location. As for range compression, $|h(s)|^2$ has a main lobe of width $\delta s = 1/B_D$, where $B_D = f_R S$ is called the Doppler bandwidth. The time S is the time during which the target is in view of the beam. It is sometimes referred to as the SAR integration time, as the azimuth correlation operation is an integral operation performed over the duration S. It can be expressed as a function of the size of the footprint in the azimuth direction $R_C\theta_a$ and the platform velocity V_S:

$$S = \frac{R_C\theta_a}{V_S} = \frac{R_C\lambda}{V_S l} \tag{2.12}$$

The azimuth time resolution is given by the width of the main lobe: $\delta s = 1/f_R S$. It corresponds to the azimuth resolution $\delta x = V_S.\delta s$. Combining this expression and Equations (2.10) and (2.12) yields the following expression for the azimuth resolution:

$$\delta x = V_S\frac{\lambda R_C V_S l}{2V_S^2 R_C\lambda} = \frac{l}{2} \tag{2.13}$$

The azimuth resolution for a SAR is in theory equal to half the length of the radar antenna. This is the originality of the processing, which actually synthesises

an aperture the size of the beam footprint in azimuth. For ERS, the SAR antenna is 10 m long, giving a theoretical azimuth resolution of 5 m. In practice, the resolution is further degraded by imperfections in the processing.

In this chapter, many aspects of the SAR processing have been ignored, such as the range migration effect and all the additional features linked to the digital processing of the signal. However, the idea here was to give indications on how very high resolution can be achieved with SARs, and therefore why it is now so widely used in the remote sensing community.

2.2.3 Basic properties of SAR images

Geometric properties

It was shown in the previous section that the resolutions of a SAR system differ in range and in azimuth. The first implication of this is that the features displayed on a SAR image will not directly map onto surface features, but will appear to be stretched in the azimuth direction. It is not in itself a major problem but can cause difficulties in the visual interpretation of the images. A common technique to remove this distortion is to average pixels along the azimuth direction. For example in the ERS case, with a resolution of about 5x25 m, averaging 5 pixels along azimuth will leave an image with "square" pixels of 25x25 m. However, averaging is done at the expense of resolution, so it should be confined to visual interpretation of the images only, and not used for data processing.

SAR images are affected by a number of other defects. Unpredicted changes in the amplitude and/or phase of the returned echo occur due to uncompensated antenna motion or unpredicted changes in the measured range. The latter can be due for example to variations of the atmospheric refractive index. The resulting effects on the image are radiometric distortions, geometrical distortions, image defocus. A detailed description of these defects and their correction can be found in [21]. Target ranging errors occur in high relief areas. The range being determined by the two-way propagation time between the antenna and the target, a variation in height between two points will result in the SAR image in a range estimation error. A point at a higher elevation will be seen by the radar at a closer distance to a neighbouring pixel of lower altitude than it actually is. This effect is called foreshortening when the slope between the two points is less than the radar look angle. When the slope is so important that it is greater than the radar look angle, there is an inversion of the two points in the radar image, and this effect is referred to as layover. The inverse problem to layover is shadowing, where a whole portion on the ground surface is not visible from the radar. Layover and foreshortening are visually obvious in SAR images of mountainous areas, where the mountains seem to lean towards the sensor.

Statistical properties

Figure 2.5 is an example of a SAR image obtained from ERS-1. The noise-like aspect of the image is due to the phenomenon of speckle. It was stated in section 2.2.1 that the total backscatter signal received by the radar antenna is the result of the summation of multiple individual scattering elements in the scattering vol-

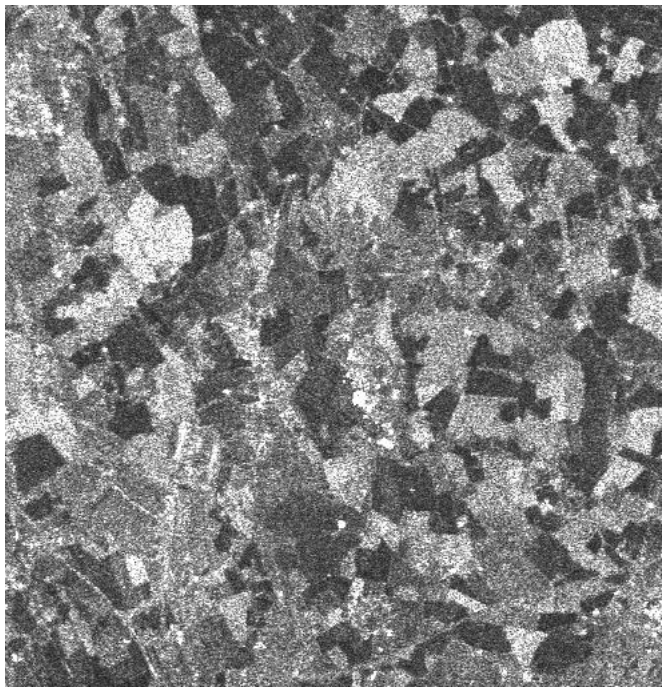

Figure 2.5: SAR image from ERS-1 of Cranfield University and its surroundings

ume. Each ground resolution cell can be viewed as containing a high number of discrete scatterers, each of them contributing to the total backscattered wave. In a mathematical form, this total backscatter signal V can be expressed as:

$$V = |V|e^{j\phi} = \sum_{k=1}^{N} |V_k|e^{j\varphi_k} \tag{2.14}$$

where $|V|$ and φ are respectively the total backscatter signal amplitude and phase, and $|V_k|$ and φ_k are the individual amplitude and phase contributions from each scatterer in the ground resolution cell. This summation is therefore comparable to an interference phenomenon between the individual contributions.

It can be assumed that the individual scatterers are in very high number in the scattering volume, so it is not physically possible to account for their individual contributions. Therefore statistics must be introduced at this stage to derive probability density functions for $|V|$ and φ. If the individual scatterers are considered to be uniformly spatially distributed in the ground resolution cell, then the phase φ is uniformly distributed over [-π,π], as the size of the resolution cell (of the order of metres) in much larger than the wavelength (of the order of centimetres). With such a phase distribution, the summation of Equation (2.14) is equivalent to a random walk in 2 dimensions, and the real and imaginary components $|V|\cos\varphi$ and $|V|\sin\varphi$ have a Gaussian distribution. The resulting backscatter amplitude therefore has a Rayleigh distribution $P_{|V|}$ [22]:

$$P_{|V|}(v) = \frac{2v}{\sigma}\exp\left(-\frac{v}{\sigma}\right) \tag{2.15}$$

The corresponding intensity distribution (intensity $I = |V|^2$) is a negative expo-

nential:

$$P_I(i) = \frac{1}{\sigma} \exp\left(-\frac{i}{\sigma}\right) \tag{2.16}$$

The mean value and standard deviation for the distribution $P_I(i)$ are both equal to σ, whose value depends on the individual scattering amplitudes $|V_k|$.

Comparisons between the statistical distributions predicted by this speckle model and observed data over homogeneous targets show a good agreement [21]. It is clear that adjacent pixels of a SAR image of an homogeneous region can give different values of the backscatter intensity as I follows the distribution of Equation (2.16). Speckle gives to the SAR images this noise-like aspect observable on Figure 2.5. It can be reduced by averaging several images of the same scene. The variance of the intensity obtained after averaging N images follows a 1/N decrease. This means that there is not much improvement in image quality after averaging the first few images.

Another important point to make here concerns the spatial correlation between pixels. It is necessary to introduce it here as it will be shown later that it has direct implications on the coherence statistics. Re-sampling of SAR data is necessary to translate the slant range to ground range, but it introduces some correlation between adjacent pixels [21], which means they do not provide independent information about the scene. The intensity correlation coefficient for a pixel lag k in the azimuth direction is [21]:

$$\rho_{I,a}[k] = \frac{\frac{1}{N}\sum_{i=1}^{N} I(x_i)I(x_{i+k})}{var(I)} \tag{2.17}$$

The summation is made over a certain area of interest containing N pixels, and $var(I)$ is the variance of the intensity over that area. x_i is the azimuth of the i^{th} pixel. A similar definition holds for the correlation coefficient in the range direction, $\rho_{I,r}[k]$. With SAR data, $\rho_{I,a}[k] \neq 0$ for $k \neq 0$. An example is shown on Figure 2.6, where the variation of the correlation coefficient in azimuth and range is plotted against the pixel lag k. The curves have been calculated from ERS SAR data over an homogeneous area, a wheat field in te image of Figure 2.5.

The presence of pixel correlation means that, for a rectangular block of M pixels in range and N pixels in azimuth, the number of independent pixels is inferior to MxN. It is shown in [21] that the number of independent "looks", L, can be defined as:

$$L = \frac{\langle I \rangle^2}{var(I)} \frac{MN}{\sum_{|k|<M} \sum_{|l|<N} \left(1 - \frac{|k|}{M}\right)\left(1 - \frac{|l|}{N}\right) \rho_{I,a}[k]\rho_{I,r}[l]} \tag{2.18}$$

$\langle I \rangle$ denotes the average intensity over the MxN block. As an example, the value of L calculated from the intensity correlation coefficients displayed in Figure 2.6, for a 3x15 block, is about 28. The value of L calculated here is important as it is used later to express statistics on the InSAR coherence.

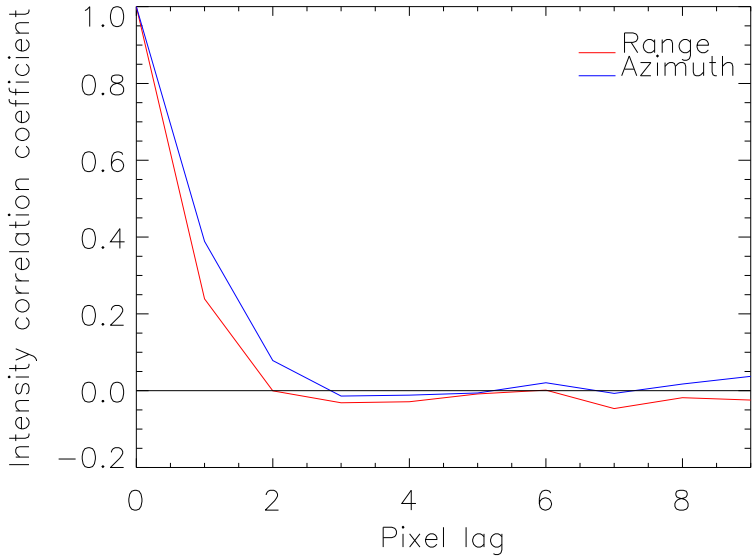

Figure 2.6: Intensity correlation coefficient on a SAR image over a wheat field, in range (red) and azimuth (blue)

ERS SAR data formats

The two main data formats available for the ERS SAR in the image mode are called PRI (Precision Image) and SLC (Single Look Complex).

The precision image is formed with three sub-images (three looks). The combination of three images is made at the expense of resolution, but the speckle effect (discussed later in this chapter) is reduced. The SAR data in PRI format is resampled to obtain a pixel size of 12.5 x 12.5 m.

Single Look Complex (SLC) format The SLC format keeps both the intensity and the phase information contained in the backscattered pulses. SLC data is necessary for interferometry applications as it retains the phase for each pixel. It is the data format used in the research.

2.2.4 SAR interferometry and the complex degree of coherence

The principles of SAR interferometry are detailed in this section, together with the parameter which is one of the main concerns of this thesis: the complex degree of coherence, commonly referred to as the coherence.

Principles of SAR interferometry

The speckle model presented in the previous section pointed out that the phase of a single pixel is uniformly distributed and therefore the phase information in individual SAR images is of no practical use. However, the phase difference between correspondent complex pixels from two SAR images of the same scene carries useful information on the relative height between two adjacent pixels.

SAR interferometry requires two views of the same scene taken from a slightly

different angle. The two ways to achieve this are (1) to carry two SAR antennas on the same platform or (2) to view the same scene with the same SAR antenna at two different times. The first solution is used with airborne SAR antennas being placed on each wing of an aircraft. With spaceborne SAR however, the second option is mostly used (at the very recent exception of the Shuttle Radar Topographic Mission), and leads to repeat-pass interferometry. For example, while in their Tandem mission phase, the ERS satellites took images of the same scene with a 24 hour time interval. The geometry for SAR interferometry is presented in Figure 2.7 in the simplified case where the Earth's sphericity is not accounted for. This simplified case is presented here because it is sufficient to introduce the issues which are the subject of later sections. A complete treatment of the problem would need to include the sphericity of the Earth and some satellite orbit errors [23].

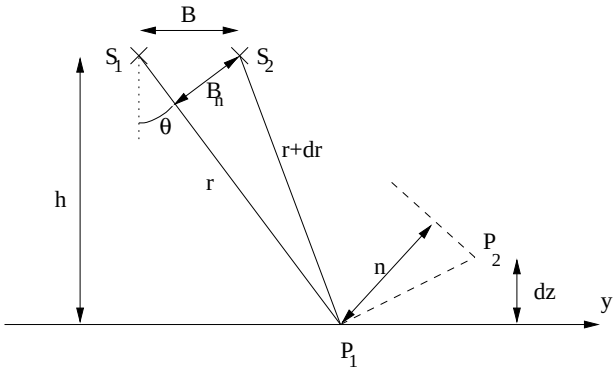

Figure 2.7: Geometry and parameters for SAR interferometry ('flat Earth' case)

The two satellites S_1 and S_2 are separated by a distance B called the baseline. B_n is the baseline normal to the direction of the radar beam. S_1 sees the pixel centre P_1 at a range r, and S_2 sees the same pixel centre at a range $r + dr$.

The interferometric phase ϕ is the difference between the phases recorded from P_1 by the two satellites:

$$\phi = \frac{4\pi}{\lambda} dr \tag{2.19}$$

The knowledge of the interferometric phase for a single pixel is of no use because, as $dr \gg \lambda$, there is an ambiguity in ϕ of many cycles. However, the variation of interferometric phase between two adjacent pixel centres, $\Delta\phi$, can be related to the surface topography:

$$\Delta\phi = \frac{4\pi}{\lambda} \Delta(dr) = \frac{4\pi B_n n}{\lambda r} \tag{2.20}$$

In this equation, n represents the displacement between P_1 and P_2 normal to the slant range direction. n depends on the distance in the y direction and on the relative elevation dz. The term related to the y direction can be subtracted from the interferometric phase variation, as it is a linear variation corresponding to a flat Earth case. The resulting phase difference $\Delta\phi_z$ due to the elevation difference dz has the following expression:

$$\Delta\phi_z = \frac{4\pi B_n dz}{\lambda \sin\theta} \tag{2.21}$$

This shows that, for a given configuration of the satellites, the interferometric phase variation between two adjacent pixel centres is proportional to the height difference between these two centres. SAR interferometry can therefore be used to generate topographic maps (DEMs). The phase values being retrieved from complex numbers, they can only be determined modulo 2π. The interferogram, which is an image of the interferometric phase across the scene of interest, therefore shows interferometric fringes. Note that, in the case where no relief is present, the slant range difference *dr* increases continuously (but not linearly) with increasing slant range. So an interferogram generated from a flat surface will also show interferometric fringes, parallel to the azimuth direction.

DEM generation is not as simple as it may seem from the simple theory presented here. It requires robust phase unwrapping algorithms, atmospheric effects are not negligible and high accuracy DEMs require the combination of data from ascending and descending passes or even combination between radar and optical DEMs (generated by stereoscopy). In addition to these problems, several factors will contribute to modify the measured phase, which are not directly related to terrain height and consequently decrease the accuracy of the DEM. The quality of an interferogram can be estimated and is quantified by a parameter called the degree of coherence.

Definition of the complex degree of coherence

The issues introduced above have been studied in the optical domain long before the radar interferometry did even exist as a discipline. It is therefore not surprising to find the roots of the concept of coherence in the studies of light interference. It was introduced to account for the fact that the phase and amplitude of real light sources undergo irregular fluctuations such that there is no correlation between the signals taken at a time t and $t+\Delta t$. The time Δt after which no correlation is found is introduced as the coherence time [24]. Obviously, between the cases when light sources are fully coherent and when they are totally incoherent, there is a whole range of partially coherent cases. The amount of coherence between light sources is directly related to the contrast of their interference pattern, and from here it was necessary to introduce a variable which would represent this amount of coherence. The degree of coherence was defined for that purpose.

For SAR interferometry, the coherence is also of interest as it quantifies the feasibility to make interferometric measurements from an interferogram. The complex degree of coherence defines the capacity of two wave fronts to stay correlated. It is defined as:

$$\gamma_c = \frac{\langle V_1 V_2^* \rangle}{\sqrt{\langle |V_1|^2 \rangle \langle |V_2|^2}} \tag{2.22}$$

where V_1 and V_2 are two wave fronts received by the satellites at their two different positions S_1 and S_2 respectively. The degree of coherence $\gamma = |\gamma_c|$ is a number between 0 and 1 directly linked to the visibility of the fringes. If γ=1, the

2 signals are perfectly coherent and the fringe visibility is maximum. If γ=0, the 2 signals are incoherent and there is no interference between them.

Qualitative understanding of the coherence

Going back to the notation introduced in Equation (2.14), the signals V_1 and V_2 received from the same area by the radar at its two different positions can be written:

$$\begin{aligned} V_1 = & |V_1|e^{j\varphi_1} = |V_1|e^{-\frac{4\pi}{\lambda}r_1}e^{j\psi_1} \\ V_2 = & |V_2|e^{j\varphi_2} = |V_2|e^{-\frac{4\pi}{\lambda}r_2}e^{j\psi_2} \end{aligned} \tag{2.23}$$

Here the phase φ_i (i=1,2) is decomposed into:

- a "travel" phase $4\pi r_i/\lambda$ corresponding to the optical path of the radar wave travelling a distance equal to the range r_i,
- a "random" phase ψ_i which, with the speckle model introduced above, is uniformly distributed in the interval [0,2π].

If the phases ψ_1 and ψ_2 are too different from each other, they corrupt the useful phase signal $4\pi(r_2 - r_1)/\lambda$ (=ϕ as defined in Equation (2.19)), and the interferometric phase does not provide useful information. The interferogram does provide information about the topography if the phases ψ_1 and ψ_2 do not differ significantly.

The coherence defined in Equation (2.22) quantifies this amount of difference, and can therefore be viewed as a quantitative indicator of the change which has occurred in the scene between the two passes of the radar antenna.

Estimation of the coherence from SAR data

Coherence is not as such *measured* from SAR data, but *estimated*. Given that the azimuth and range coordinates correspond to temporal coordinates of the sampled radar signal (see section 2.2.2), the most frequently used coherence estimator is [10, 25]:

$$\gamma = \frac{\left|\sum_{i=1}^{M}\sum_{j=1}^{N} s_1(i,j)s_2^*(i,j)\right|}{\sqrt{\left(\sum_{i=1}^{M}\sum_{j=1}^{N}|s_1(i,j)|^2\right)\left(\sum_{i=1}^{M}\sum_{j=1}^{N}|s_2(i,j)|^2\right)}} \tag{2.24}$$

with $s_1(i,j)$ defined as the complex pixel values of the first image in a MxN pixel calculation window, and $s_2(i,j)$ the corresponding values in the second image. Note that there are other coherence estimators which have been reviewed and compared in [26].

Coherence statistics

Equations (2.15) showed that the amplitude of a complex pixel in a SAR image is a statistical quantity following a Rayleigh distribution, while the phase of the pixel is uniformly distributed. Since, by definition, the coherence is a function of these complex pixels on a given area, it can be expected that the coherence estimator of Equation (2.24) is also a statistical quantity. The probability density function of the coherence estimator γ is derived in [27], and from it, the expected value of γ, E(γ), can be expressed as a function of the true value of the coherence magnitude γ_{true} and of the number L of independent samples in the coherence calculation window. The mathematical formalism is not reproduced here to avoid adding unnecessary complexity but a full derivation can be found in [27]. Figure 2.8 shows the probability density function of γ for a true coherence magnitude $\gamma_{true} = 0.5$, and for 3 values of L (3, 10, and 20).

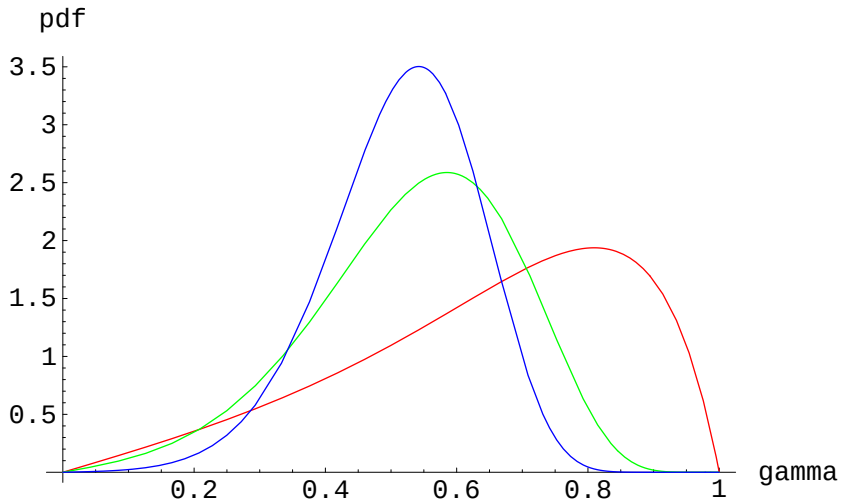

Figure 2.8: Probability density function of γ for γ_{true}=0.5 and L=3, 10, and 20 (red, green, and blue respectively)

It is clear from the shapes of Figure 2.8 that the expected value of γ calculated from the probability density functions will be higher than γ_{true}. It is also clear that, in order to obtain a good estimation of the true coherence, a larger calculation window should be chosen. This, however, is made at the expense of spatial resolution on the coherence image and also requires that the calculation window covers an homogeneous area on the ground. In practice, a compromise is made between good spatial resolution and reliable estimation of the coherence. Another way to view this result is shown in Figure 2.9, where E(γ) is plotted against γ_{true} for 3 values of L (5, 10, and 50). E(γ) is higher than γ_{true}, and especially so at low coherence values. This phenomenon is known as coherence bias. As it will be shown later, coherence above vegetated surface is by nature fairly low, so it is important to remove the bias in the coherence estimates calculated from Equation (2.24).

A reliable method for bias removal was proposed in [28]. It consists of calculating the coherence estimator from Equation (2.24), and averaging the values obtained over an area of interest:

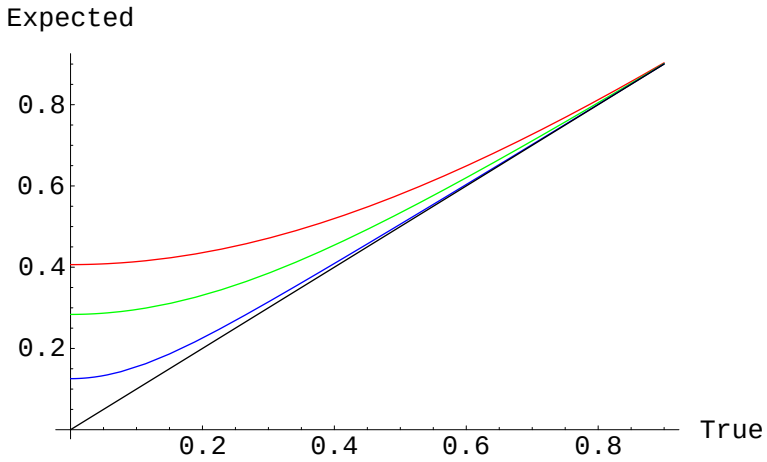

Figure 2.9: Expected value E(γ) as a function of the true coherence value for L=5, 10, and 50 (red, green, and blue respectively)

$$\bar{\gamma_L} = \frac{1}{n_{AOI}} \sum_{i=1}^{n_{AOI}} \gamma_{Li} \tag{2.25}$$

The area of interest (AOI) can be for example a field, and in general any homogeneous area on the surface. The average coherence is taken over its n_{AOI} pixels and, in Equation (2.25), the subscript L denotes that the coherence was calculated from L independent samples. It is shown in [28] that the spatial average $\bar{\gamma_L}$ provides an unbiased estimate of the expected value E(γ) over the AOI. The mathematical relation between E(γ) and γ_{true}, which was used to make the plots of Figure 2.9, can then be inverted numerically to provide an unbiased estimate $\hat{\gamma}$ of γ_{true}. Obviously $\hat{\gamma}$ is not strictly equal to γ_{true} since the spatial averaging was performed with a limited number of pixels. In theory, with an infinite number of pixels, $\hat{\gamma}$ would tend towards γ_{true}. With the unbiased estimate $\hat{\gamma}$ comes a certain number of statistics, including the definition of confidence intervals. To conclude on this point it should be noted that further coherence statistics and bias removal techniques can be obtained under other assumptions. In particular, techniques have been developed [28] when the scatterers are assumed to be unevenly distributed in the ground resolution cell (non-stationary processes).

2.2.5 Decorrelation factors

The loss of coherence is referred to as decorrelation, as the coherence magnitude is effectively a correlation coefficient between the two complex SAR signals. It is commonly decomposed into 3 components, namely the thermal, spatial, and temporal decorrelation [29]:

$$\gamma = \gamma_{thermal} \cdot \gamma_{spatial} \cdot \gamma_{temporal} \tag{2.26}$$

Decorrelation could *a priori* be considered as an unwanted effect which infers information loss on an interferogram. Although this is true for DEM generation,

it will be shown in this section that decorrelation is also at the basis of additional information about the surface.

Thermal decorrelation

Thermal decorrelation is associated with the noise introduced in the SAR processing. The coefficient $\gamma_{thermal}$ is related to the signal-to-noise ratio (SNR) by [29]:

$$\gamma_{thermal} = \frac{1}{1 + SNR^{-1}} \tag{2.27}$$

Spatial decorrelation

The spatial decorrelation is also known as baseline decorrelation. It was first introduced in [30], and a more complete description can be found in [31]. Baseline decorrelation is a geometric effect due to the fact that there is a change of viewing angle on a fixed surface point, due to the distance (the baseline) separating the radar antennas. This difference in the viewing angles is small but it infers a change of the relative positions of the scatterers in the ground resolution cell. Consequently the two radar antennas measure different values for the range (and associated phase) of these scatterers, and the complex addition of all the individual contributions in a resolution cell will lead to a different resulting amplitude and phase measured by the two satellites. Expressed in other words, changing the viewing angle is equivalent to changing the interference pattern in the pixel. If the difference in viewing angle becomes too important, all coherence is lost and $\gamma_{spatial}$=0. This last point introduces the idea of a maximum distance between the two satellites for SAR interferometry to be possible. This distance is named the critical baseline. The variation of $\gamma_{spatial}$ as a function of the baseline has been calculated in [31]. With the ERS parameters, the critical baseline is approximately 1100 m.

When the baseline is inferior to the critical baseline, the decorrelation effect can be removed from the coherence images using a technique known as common band filtering, which relies on the concept of wavenumber shift [32]. Because of the difference in viewing angle between the two satellites, the projection of the wavenumber k ($k = 4\pi/\lambda$) on the ground surface, k_g ($k_g = 4\sin\theta/\lambda$) takes different values. The ground range wavenumbers are therefore slightly shifted. Consequently, the backscattered signals are different because the incoming signal does not exactly excite the same spectral components of the ground reflectivity spectrum. The bandwidths of the two backscattered signal are shifted, and the idea of the common band filtering technique is to keep only the part of the spectra which is common to both signals.

It should be noted that additional spatial decorrelation should exist due to rotation of the look directions between the two radar passes [29]. With spaceborne SARs, this effect is negligible as the spacecraft orbits are precisely controlled and kept parallel to a very good accuracy.

Temporal decorrelation

Temporal decorrelation is specific to repeat-pass interferometry, and occurs because of a change of the scattering properties of individual scatterers on the surface. Change in these properties can have different sources, depending on the time interval between the two radar passes. Different time scales can be considered to account for the change of scattering properties in a vegetation medium:

- at short time scales (seconds), the wind can move the scatterers (leaves, stalks, etc...) in a random manner. This results in a different scattering configuration between the two satellite passes of the interferometric pair.

- At medium time scales (hours, days), the dielectric properties of the scatterers can be affected by rain and temperature transitions (ice/ liquid water).

- At long time scales (weeks, months), the scattering properties change due to crop growth, man-made changes (harvest, ploughing, sowing, etc...), and possibly exceptional events (floods, fires, etc...)

It can be expected that temporal decorrelation will be higher in forested and agricultural areas, and virtually non-existent in built-up areas. This is the very important property that is going to be exploited in this report.

In the case of the ERS-1/2 tandem mission, where the time difference between the two images is only 24 hours, it is expected that temporal decorrelation is mainly due to a change of the position of the scatterers in the ground resolution cell. Changes in moisture can also occur in case of rain events between the two satellite passes. At C-Band (f=5.3 GHz, λ=5.67 cm), a motion of the scatterer of a few centimeters results in the phase change of one cycle or more. Therefore, one-day coherence calculated from the tandem mission data is expected to be sensitive to vegetation structure. As the plant grows over the season, its structure changes and so does its random motion between the two satellite passes. The temporal variation of the coherence over the growth season for a given crop should reflect this structural change. It is in this respect that the temporal decorrelation can be viewed as a useful source of information about the surface and volume processes which affect the stability of the observed scene.

2.3 Use and limitations of InSAR coherence for vegetation remote sensing

From the properties shown in the previous section, it is clear that the coherence presents an interest for the remote sensing of vegetated areas. This section reviews the research done to this date in this direction. From the review, a certain number of limitations will be identified, and some of them will be used to drive the definition of the objectives of this research.

2.3.1 Current applications of the coherence

The information contained in the temporal decorrelation was first acknowledged qualitatively in [29], where the coherence over forested areas was found to be inferior to a reference bare surface. In [31], the effect of rain, freezing, and wind is also acknowledged to have an impact on the coherence. These two studies simply stated the expected causes of temporal decorrelation without making a quantitative use of it. It is interesting to note that [29] and [31] were published in 1992 and 1995 respectively, which shows that the quantitative study of coherence is a young area of research.

A more quantitative step was then taken, especially in forestry applications. In [33] the coherence derived from ERS-1 InSAR observations is plotted against the forest stem volume. A modelling approach is proposed, making use of a simple backscatter model and assumptions about the amount of temporal decorrelation from trees. The two important points made in [33] are:

- "*of the various decorrelation phenomena, [...]the wind decorrelation is most important, acting on time scales of minutes and shorter*"
- "*the model assumptions are suffering from lack of observation or accurate observations of some parameter values*"

The same research group shows in [34] that some good correlation is found between coherence and forest biomass. However, there is a high variability in the correlations made at different dates, and the weather conditions again are put forward to justify this variability. Again, the need for additional research on how these weather conditions affect the coherence is acknowledged. The temporal variation of coherence over forested areas in presented in [35]. Discrimination of tree type using the temporal trace is shown to have some potential, but more interesting in the paper is the first graph showing the variation of coherence over a forested area against measured wind speed at different. The observed decrease of coherence with increasing wind speed is the first experimental proof of the dependence of the two parameters. However, in [36], the coherence calculated over forest is reported to be independent of wind speed. The explanation given is that even low wind speeds are enough to make the trees move significantly and destroy totally the coherence between the two SAR signals.

Another application is presented in [10, 11]: the coherence is one input parameter in the generation of land-use classification maps, alongside the backscatter intensity and the backscatter difference. 8 classes are derived on the map and the overall accuracy of the classification is about 80%. The sensitivity of coherence to man-made changes such as field harvesting and ploughing is stated, and the first published plot of coherence against soil cover fraction for a crop field shows an almost linear decrease between the two parameters. Finally, [11] recognises the potential use of the temporal variation of the coherence throughout the growth season to differentiate crop types.

Moving on specifically to agricultural applications, [13] is the first attempt to relate the coherence to crop height, using a time-series of ERS-1/2 Tandem data, for which the time difference between the two satellite passes is one day. To this

day, [13] uses the most complete data set of crop data and SAR data with a view to study the potential use of coherence as a useful parameter for agricultural studies. The decrease of coherence with increasing crop height is observed, and modelled by a simple decreasing linear relationship. However, the standard deviations on the coefficients is far too high to use reliably these linear relations to retrieve the crop height. The poor accuracy of the modelling is mainly due to the high variability of the coherence measurement, related once more to the changing weather conditions. An interesting study presented in [13] shows the temporal variation of the coherence throughout the growth season for different types of crops. The variations, specific to each individual type confirms the conclusion of [11] that crop differentiation is potentially achievable from coherence measurements.

A similar study using a different data set is presented in [14, 15]. The decreasing linear relation between coherence and crop height for different types seems to yield better results than in [13], with a maximum difference between the modelled and the true wheat height of 22% . Classification of crop types with several methods, including the use of the temporal variation of coherence, did not yield satisfactory results in [15].

All the studies quoted above have in common that they use the qualitative understanding that the coherence is related to vegetation parameters such as forest biomass, crop height, wind speed. Indeed it can be expected that a crop field or a forest stand higher than its neighbours will have a higher sway amplitude in the wind and therefore should contribute more significantly to the temporal decorrelation. However, none of these studies accounts for the amount of decorrelation because they are not based on a quantitative understanding of the physical mechanisms relating the temporal decorrelation to some vegetation parameters and the wind.

2.3.2 Coherence modelling

In [8] the coherence is modelled as the complex sum of a ground component and a vegetation component. The complex vegetation component of the coherence has an amplitude which is a function of the contribution to the total backscatter intensity from the vegetation layer. The phase of the vegetation component of the coherence is an empirical function of the wind speed and the forest type. The vegetation component is added to a ground component whose phase is set to 0 and amplitude is determined by the ground contribution to the total backscatter intensity. The different parameters of this model are chosen so they fit the coherence obtained from ERS SAR data. The conclusion of the study presented in [8] is that the forest coherence model is qualitatively in agreement with the measured coherence. This is a positive point as it shows that the modelling approach is capable of yielding sensible results. However, the calibration of the model requires simultaneous SAR data and ground data about the surface. In addition to this, the influence of wind speed and forest type is represented in the model by a single coefficient which can be viewed as a "black box" accounting for phenomena which are not physically understood between wind and tree swaying.

The works developed in [8] have been used recently in [9] to attempt to retrieve forest biomass. The result of this study is that forest biomass retrieval via the

modelling approach, combined with InSAR data, can compete in accuracy with the traditional techniques. However, the accuracy is not constantly competitive, especially with coherence observations in winter and in certain weather conditions.

A step further in the modelling of coherence was taken in [37], where the scattering volume is modelled as a cloud of small particles. The temporal decorrelation is simulated by giving to each particle in the volume a statistical position defined by a Gaussian distribution. The coherence is calculated by coherent addition of the contributions from all particles. Here, the modelling includes some description of the motion of the scatterers through the introduction of statistical distribution of the scatterers position. The model is used in [38] to retrieve tree height from observations. Overall, the results are accurate but large differences are found in the most windy days. The author recognises in [38] that his model is inaccurate in high wind speed conditions, from which it can be inferred that the use of a Gaussian distribution may be inappropriate to describe the motion of scatterers subject to wind forcing. However, the methodology developed is valuable. The same methodology was also developed in [39] but is more general in that the scatterers can have different shapes and therefore be more representative of a real vegetation medium. In addition to this, other motions can be included, such as leaf rotation. The model simulations presented in [39] are preliminary, so their analysis is not debated here.

2.3.3 Conclusion of the use of coherence for vegetated areas: current limits

Sections 2.3.1 and 2.3.2 have shown the current state of development of the coherence over vegetated areas, both at the application and modelling levels. From the applications side, the coherence has been successfully used in different ways, and certainly proved its potential for forestry applications. The general conclusion, however, is that there are many unknowns in the way coherence can fluctuate to make it an accurate reliable tool for vegetation monitoring. The modelling side can be viewed as an attempt to understand these unknowns. Most of the difficulty to grasp the significance of temporal decorrelation originates in the lack of knowledge concerning the motion of the scatterers. Some modelling approaches avoid this problem by hiding the motion behind empirical coefficients, and some other models do take into account the random nature of this motion by introducing probability distributions. When applying their modelling approach to the forestry problems, all studies point out that the knowledge of the weather conditions is required to make their approach more valid and relevant to vegetation monitoring.

It appears from the review presented in the last sections that the use of coherence for vegetation monitoring is limited by the lack of detailed knowledge of the motion of scatterers in the scattering volume, and by how this motion relates to the weather conditions, in particular wind. Not only this lack has limited the accuracy of the potential applications in agriculture and forestry, but more importantly it has not been possible to state on the usefulness of coherence for *quantitative* use in these two applications.

The modelling approach to account for the coherence levels obtained from SAR data seems to provide valuable insights into the key parameters to consider. An

important aspect of these models is that they include some description of the motion of the vegetation. Indeed, since the random displacement of the scatterers in a vegetation medium is the cause of the temporal decorrelation, it is a necessary requirement to include them in coherent models. Since the motion of trees and crops seems to be of prime interest here, the next section reviews work done in this area.

2.4 Measurement of wind-induced vegetation swaying: state of the art

To the knowledge of the author there are no studies showing measurements of the motion of trees and crops with the specific aim to relate them to the coherence. However there have been some motion measurements made on trees and crops for other purposes. Investigations on wind-induced tree sways are important in forestry because they lead to storm damage in forests, which are an important source of economic loss. The problem of lodging for crops, particularly corn and wheat, has motivated similar studies in the agricultural research community. In addition to these economic motivations, the interactions of trees and crops with wind are the subject of studies in micrometeorology in the atmospheric boundary layer.

2.4.1 Wind-induced tree swaying

The measurement of the interactions between trees and the wind dates back to about 40 to 50 years. It is not the purpose of this section to present a historical perspective on this subject, but rather to summarise recent works in the area, and assess their advantages and disadvantages.

A very complete study of wind-induced tree sways is presented in [40]. First, the response of a tree to a dynamic wind load is modelled on a theoretical basis, taking into account the elastic properties of the trunk and the drag induced by the wind blowing on the branches and leaves. Another interesting point of [40] is the modelling of a tree as a mechanical system defined by its transfer function. The input to the tree transfer function is the wind speed and the output is the motion of the tree. From this approach, the resonant oscillating frequencies can be found. [40] also presents some simultaneous measurements of wind speed and tree motion. The motion and acceleration of the trunk only is measured at different heights. The measurement system uses sensors placed on the trunk itself.

The methodology developed in [40] is not directly transferable to crops since it uses invasive sensors which would affect significantly the motion of a crop plant. In addition to this, and bearing in mind that the knowledge of motion is to relate to the coherence, a more precise way of measuring motions is required.

The more recent study presented in [41] for identical purposes uses a similar approach. The tree is modelled by a mass-spring-damper rotary system, and its theoretical transfer function is calculated and compared to the transfer functions derived from measurements of wind and motion. The motion of stems is measured by tilt sensors placed on the tree itself. Again, the methodology is not directly trans-

ferable to crops because it is invasive and would change the mechanical properties of the plant.

Other studies have been made, including some analysis in a wind tunnel, and detailed analysis of the turbulence with the tree canopy [42]. They are not detailed here because the two analyses quoted above represent a good summary of the state of the art in terms of wind-induced tree-swaying. The methodology is interesting, but does not directly apply to crops.

2.4.2 Wind-induced crop swaying

The motion of corn is analysed in [43]. The wind speed is measured simultaneously with the corn motion. The displacement is measured with a joystick, which is actually a robotic arm in contact with the corn stalk. The spectral method is used again to describe the corn motion and gives good insights into the physical mechanisms inducing the motion. It shows a peak oscillating frequency of about 1 Hz, and some other features related to the growth stage of the corn. The study also points out the complexity of the motion: for example, its main direction does simply relate to the wind main direction because of the turbulence effects at the crop canopy level. The drawback of the study presented in [43] is that the displacement measurement is made with a sensor requiring contact with the crop, which therefore may modify significantly its movement.

An earlier study published in 1978 [44] did overcome that difficulty by measuring the motion of plants with an 8 mm cine-camera, in conjunction with wind measurements from anemometers. The measurement technique was therefore better in principle because non-invasive. However, the analogue outputs of the recording system made the data processing long and tedious. But the methodology of [44] is nevertheless very sound.

Other studies like [45] have presented wind measurements in a wheat field, together with some motion measurement data. However these studies were motivated by the investigations on wind turbulence on its own, rather than for dedicated analysis of wind-crop interactions. For that reason, they are not detailed here. However they provide useful sources of wind data, and crop motion data.

2.4.3 Conclusion on the vegetation swaying studies

The several techniques used in the studies presented above are very valuable because they have shown the available measurement techniques. The potential of the methodologies developed is expressed in terms of accuracy of the wind and motion measurements, and more importantly of the relationships that can be derived between the two. The main conclusions to draw from the publications listed in the previous sections are:

- The simultaneous measurements of wind speed and tree or crop motion do provide insights about the detailed interactions between the two, with a good accuracy in terms of short time scale mechanisms and measured displacement.
- Using contact sensors to measure displacements is applicable to trees but not to light crops.

- The complexity of the crop motion in the wind is well acknowledged. This is to balance against the rather simplistic motions assumed in the coherent models (see Section 2.3.2).

- Most of the crop displacement measurement techniques require specialised (and therefore expensive) equipment which is not always easily transportable and therefore not well adapted to field measurements.

2.5 Objectives of the research and methodology

Several points have been made in Sections 2.1 to 2.4 which have a direct impact on the definition of the objectives of the research. They need to be recapitulated briefly so the objectives and the methodology described later in this section make sense. It is the purpose of the following section to make this recapitulation, after which the research objectives are stated, the tools to achieve these objectives are presented, the methods to use these tools are reported, and finally the expected outputs of the research are described.

2.5.1 Summary of the important issues raised in the previous sections

The previous sections have introduced the general issues of prime interest for the remote sensing of vegetation from SAR data. The physical understanding of SAR data and of coherence is directly related to the configuration of the scattering elements within the canopy. This configuration is usually modelled by some statistical properties, either to describe the random orientation and position that these scatterers can take, or to account for the variability of their scattering properties which is linked to the meteorological conditions (wind and rain mainly, but also temperature). Any statistical description of a complex medium will necessarily introduce some simplifications which drive the accuracy of the models. Past studies have shown that a simplistic statistical description of the motion of scatterers lead to inaccurate coherence prediction from the models. Similarly, overly simplistic statistical descriptions of a vegetation medium will lead to inaccurate predictions of the backscatter intensity.

The need to have measurements of crop motion in parallel with some wind measurements arises from this necessity to understand the physical mechanisms leading to decorrelation, but also influencing the backscatter intensity. Providing these measurements is in itself valuable for a range of other users. The measurements can be used by developers of radar backscatter intensity models and coherent backscatter models, but also to assess the potential of coherence for agricultural and forestry applications.

A review of the current techniques used to make measurements of tree or crop motion has shown that most of them are either demanding in terms of equipment, or too invasive to account for the motion of plants in their true natural environment. Some means to make these measurements at low-cost, with accuracy, and with an easily transportable system, are required. Only with such a system can the

measurements be easily repeated and therefore made in a wide range of weather conditions, for different vegetation types.

Finally, one of the first points made in section 2.1 should be repeated here. Wind and motion measurements should benefit to the current understanding of coherence, but it should be kept in mind that this understanding is for the end purpose to use coherence in operational applications. For that reason it is important to illustrate, at least in a limited number of cases, how an improved physical understanding of the coherence links to real applications.

2.5.2 Objectives of the thesis

The objectives of the research are formulated as follows:

1. *Objective 1*: a database of three-dimensional crop motion throughout the growth season should be created, together with simultaneous measurements of wind velocity. The aim of this database is to be used for SAR applications, but can in principle be used for other studies such as the problem of crop lodging or the analysis of crop-wind interactions for micrometeorology. The research will be limited mainly to the study of wheat.

2. *Objective 2*: in order to provide the database, a measurement system will be designed, with a particular emphasis on its low cost, portability, and short data processing time.

3. *Objective 3*: the measurements will provide relationships between wheat motion and wind velocity.

4. *Objective 4*: It will be shown how these relationships can be used to relate to the study and understanding of the temporal decorrelation. The potential of coherence to monitor wheat will be assessed from this new understanding. In particular, the operational impact of the radar wavelength, resolution, repeat-pass time will be linked to the coherence expected from wheat fields.

To the knowledge of the author, there is no currently available data set of wheat motion and wind velocity collected throughout an entire growth season. For that reason the first objective of the research presents some novelty. And so does the second objective stated above, as a measurement system of three-dimensional displacements is not readily available from the market, especially for a reduced cost. The third and fourth objectives of the thesis can be viewed as a logical product of the first two. They are important because it is necessary to show that the measurements made have a real value for model application development. But it is mainly expected that the measurements produced during the research will provide an unequalled data source for full-time SAR model makers and applications developers.

2.5.3 Available data, software, and hardware

The following list is a very brief overview of the tools used in the research to meet the objectives described above. They will be the object of a more detailed description

in subsequent chapters of this report. It is however necessary to give here an idea of the resources available for the project and how they relate to the research objectives. The tools used during the research are:

- Cranfield Automatic Weather Station (AWS) data: the AWS continuously takes records of wind speed, wind direction, temperature, rainfall at Cranfield University since 1996. It is a valuable source of information to derive statistics about wind conditions, rain conditions on a yearly basis for an area which is assumed to be typical of South-East England.
- ERS-1/2 Tandem mission data: there are 15 pairs of SAR SLC data available for the area surrounding Cranfield. The data were acquired between June 1995 and May 1996. They are used to generate time-series of coherence data over specific regions.
- ISAR software: ISAR is a software which generates the coherence image from two SLC images. It was developed by Politecnico di Milano, Italy, for ESA-ESRIN [46].
- Erdas Imagine is used for visualisation and SAR image processing.
- Digital Vane Anemometers (DVA): these anemometers are used to make the wind measurements at the wheat canopy level. The associated circuitry and connecting cables are also available. The entire equipment is described in Chapter 5.
- Digital video cameras and associated hardware for data acquisition (described in Chapter 4). The video cameras are used to measure the motion of wheat.
- Software associated with the video equipment for data processing.

2.5.4 Content of the remainder of the report

Since the justification of the research finds its roots in the modelling of coherent backscatter, it is also the starting point of the research. A coherence model is necessary to meet objective 4 described above. Its basis was already available at Cranfield University [47], and is described in Chapter 3, together with the RT2 backscatter intensity model [48]. It is shown in Chapter 3 how RT2 and the coherence model are used in conjunction with each other for agricultural applications. The use of the models will help to define some system specifications, in particular in terms of the accuracy of the necessary wheat motion measurements. Then the experimental setup can be described. Chapter 4 describes the equipment used for the retrieval of the position in three dimensions of moving targets. Chapter 5 describes the anemometry package. The simultaneous use of the two measurement systems is explained in Chapter 6, and the results of the measurements are presented. In Chapter 7, the measurements are used to modify the initial coherence model presented in Chapter 3 and to support the discussion about the potential use of the wheat motion information for modelling purposes and the potential operational use of coherence for agricultural applications.

Chapter 3

Radar backscatter and coherence modelling over agricultural crops

The purpose of this chapter is to present the outputs of a backscatter intensity model, RT2, and of a coherence model over agricultural surfaces. The modelling of backscatter intensity from crops is not the prime concern of the research, but it is necessary to introduce it here in order to have an insight into the backscattering mechanisms as they directly relate to the levels of coherence observed. For that purpose, section 3.1 presents a brief introduction to radar backscatter modelling over vegetation and to the RT2 model. Outputs related to vegetation modelling are given in sections 3.2 and 3.3. The objective of these two sections is not to provide a detailed analysis of the backscatter intensity from crops, but to introduce the parameters which have an effect on it. The interpretation of the outputs of the RT2 model are used to state on the most adapted SAR configuration for the operational use of crop monitoring, from the backscatter intensity point of view. The main reason to present the RT2 backscatter intensity model is that it also models the separate contributions to the total backscatter from the different parts of the vegetation layer. This feature is of prime importance in the modelling and understanding of temporal decorrelation and is for that reason very relevant here. Section 3.4 presents a coherence model and discusses its assumptions, strengths and weaknesses. Some sample outputs are given in section 3.5. They are interpreted and show the need to have some real *in situ* measurements of crop motion. Some measurement specifications derived from the model outputs are given in section 3.6. They will be used to drive the design of the measurement system described in Chapters 4 and 5.

3.1 Introduction to radar backscatter modelling over crops

3.1.1 Overview of modelling approaches

The most straightforward step towards the modelling of radar backscatter intensity over agricultural fields is to derive empirical relationships from SAR observations. There is a very high number of publications following this approach and their de-

scription is beyond the scope of this report. Papers like [49] (spaceborne SAR) or [50] (airborne SAR) are two examples using this approach. In [49] the backscatter coefficient σ^0 is correlated to the Leaf Area Index (LAI) and it is pointed out that empirical relations are subject to variations of other parameters such as soil moisture. For that reason [49] states that some modelling is required in order to understand the full extent of the information contained in the empirical relationships. In [50], the author uses airborne SAR data and field measurements from a variety of crop types to assess which crop characteristics can be derived from SAR imagery after image processing techniques. The conclusion of this study is that, although some valuable relations were found in certain cases, it is difficult to make generalisations as the field measurements and SAR observations concern only a single regional area and a single growth season. In addition to this, the author points out that some of the observations give results which are contradictory with some theoretical backscatter models.

The studies of [49] and [50] are a good representation of the advantages and disadvantages of the empirical approach. On the one hand, SAR observations and ground measurements are an unequalled source of information to assess the use of SAR data for crop monitoring, and to tune the parameters of the theoretical models. On the other hand, the interpretation of the observations depends on a wide range of variables whose relative importance is difficult to assess. In addition to this, observations always concern a limited region in time and space and are therefore fairly difficult to generalise. Long term observation campaigns such as the one recently presented in [51] can overcome this difficulty, in that they provide data which can be used to assess the consistency of the SAR observations from one year to the other. But even studies such as [51] do use a modelling approach to fully understand the parameters influencing the observations.

Effective use of the data therefore requires a proper understanding of the physics driving the interactions between radar waves and crops. However, backscatter models are not the unequivocal answer to the limits of the empirical approach. Models involve a large amount of generalisations and simplifications in the description of crop canopies. Reproducible SAR observations in laboratory conditions, such as those presented in [52], provide very valuable insights into the scattering volume mechanisms.

The formulation of radar backscattering models, either from the wave theory or the radiative transfer approach, is based on a series of approximations. For surface scattering, the models usually use different approximations related to the soil roughness compared to the radar wavelength [18]. For volume scattering, the models usually define the vegetation medium with a series of simple geometrical shapes (ellipses, cylinders, etc...) representing elements of the crop or the tree (leaves, stalks, etc...). The orientation, density, size, and moisture content of these elements depend on the vegetation type. From the definition of these geometrical objects, the principles of wave theory or radiative transfer are applied from approximated solutions which depend on the relative size of the objects with respect to the wavelength. A description of volume scattering modelling is given in [53].

One of the first reported vegetation backscatter model [18] describes the vegetation as a layer containing uniformly distributed water droplets whose water content

represents the water content of the vegetation (the water cloud model). The simplicity of this model makes it useful for qualitative studies. The Michigan Microwave Canopy Scattering (MIMICS) model [54] is based on radiative transfer and originally designed to model backscatter from trees. It includes more sophisticated scattering mechanisms such as the "double-bounce" of the radar wave (from the radar to the tree trunk, to the ground, and back to the radar). The model has been widely used and adapted to backscatter modelling from crops [1]. The RT2 model is based on the same principles as MIMICS (radiative transfer) but includes more versatility in the description of the vegetation layer.

3.1.2 The RT2 backscatter modelling software

RT2 is described in detail in [48]. RT2 predicts the backscatter coefficient from a vegetation medium above a rough or specular surface. The required input parameters describe the constituents of the vegetation, the geometry of the surface, and the radar configuration. RT2 can run in two modes, namely single or multi-parameter. In the latter, one of the input parameters can be varied over a user defined range, whereas the outputs of RT2 are given for a single set of input parameters in the single parameter mode. The software is composed of three independent modules named *rtsetup*, *RT2*, and *read-and-write*.

rtsetup

This module is used to create a model input file to be used by the RT2 module. When started, rtsetup displays a window where all input parameters are entered. It allows the definition of 3 above ground layers, each with a maximum of 5 different types of scatterers. The input parameters are described in detail in Appendix A.1. rtsetup creates a model file (extension .rtm) used by the RT2 module for the calculation. A summary file (extension .sum) containing a list of all input parameters can also be created, in a simple text format.

RT2

The RT2 module uses the input parameter file created with rtsetup and calculates the backscatter coefficients for the four polarisation combinations (HH, VV, HV, VH) and the vertical penetration depths for V and H polarisations in each three layers. The output is given in a data file containing as many lines as the number of values of the varied parameter. The format of the RT2 output file is shown in Appendix A.2. In the single parameter mode, the one line output is displayed on the screen as well as written in the output file. RT2 also outputs a second file which summarises the first one in a Matrix form, named the Mueller matrix. This Mueller matrix file is needed by the third module of RT2, read-and-write.

read-and-write

This module uses the Mueller matrix given by RT2 to calculate the contributions to the total backscatter from the different layers of vegetation. Several files are created,

for each polarisation combination. The output files are composed of as many lines as the required number of values of the varied input parameter (similarly to the RT2 output file). It is composed of 14 columns, each of them giving the contribution from one of the following scattering mechanisms: direct scattering from each layer, surface scattering, double scattering between each layer and the surface, inter-layer double scattering, intra-layer double scattering. Appendix A.3 gives a detailed description of the output file format from the read-and-write module.

3.2 Radar backscatter sensitivity to crop geometry

Before modelling crops with RT2 and analyse their expected backscatter, it is first interesting to determine the important radar parameters which should be considered for the remote sensing of crops. For that purpose this section analyses the backscatter intensity predicted by RT2 for a series of radar wavelengths, incidence angles, polarisation combinations, and for different configurations of the scattering volume. The influence of stalk size and orientation is analysed. From this study, some of the key issues concerning the specific backscatter mechanisms from crops will arise. It is the aim of the analysis to retain some generality, so the scattering volumes which are to be presented in this section do not represent a particular crop, but consist of simplified geometrical shapes, where a single parameter can be varied at a time.

3.2.1 Influence of the stalk size

The radar configuration and the scattering volume specified in RT2 have the following characteristics:

- A single type of scatterer is present in the vegetation layer. It is a cylinder of radius r_c and length $l_c = 100r_c$.
- The stalk radius r_c is varied, from 0.1 to 1.5 cm, therefore covering most crop stalk sizes.
- The number density of the cylinders is such that it represents a constant biomass of 50 m^3/ha, in a vegetation layer of height h=1 m. The choice of a constant biomass neutralises the reported sensitivity of the backscatter intensity to this parameter, so the effect of the cylinder radius can be studied independently.
- The cylinder orientation is set to be uniformly distributed in a 2π range.
- Four radar frequency bands are covered: X-Band ($\lambda = 3cm$), C-Band ($\lambda = 5.6cm$), L-band ($\lambda = 25cm$), P-band ($\lambda = 66cm$). The radar incidence angle is set to 45°
- The surface is defined here with the parameters given in one of the examples of the RT2 manual [48]: its roughness is 0.001 m and its correlation length 0.15 m.

The variation of σ^0 with r_c for the 4 bands, and the VV, HH, and HV polarisations is given in Figure 3.1.

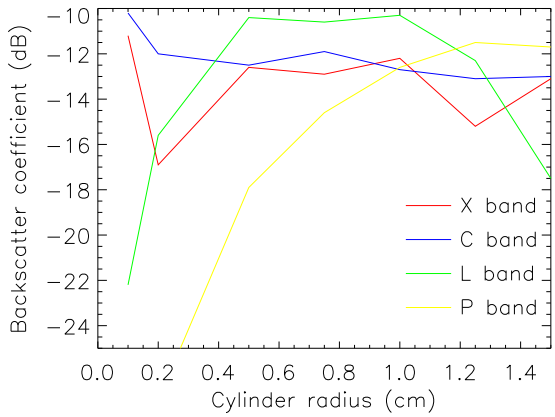

(a) VV polarisation

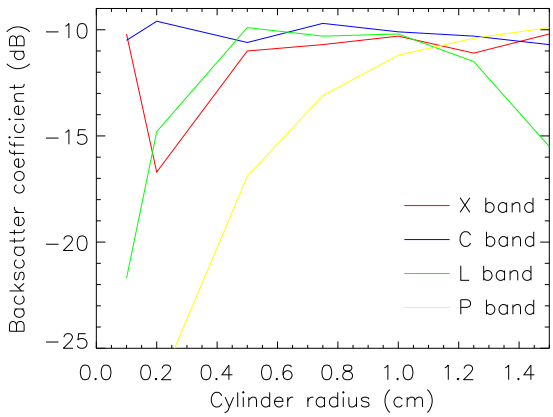

(b) HH polarisation

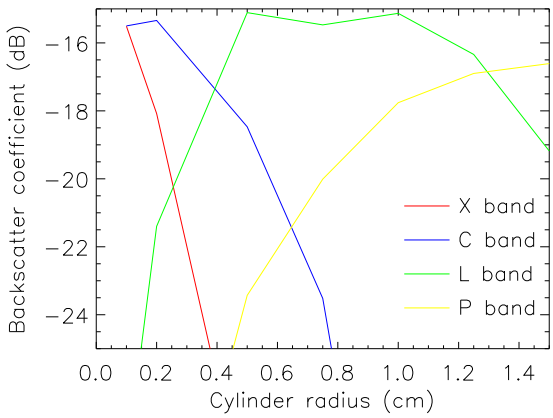

(c) HV polarisation

Figure 3.1: Variation of σ^0 with the stalk radius r_c

The variation of σ^0 for the VV and HH polarisations (Figures 3.1(a) and 3.1(b)) is similar and is jointly commented here. At P-band, σ^0 becomes significant only for larger branches ($r_c > 1$ cm). The variation of σ^0 at L-band shows that the backscatter is significant for $r_c > 0.4$ cm, but it decreases for stalk radii superior to 1 cm. At C-band the backscatter remains significant for the entire range of stalk radii represented on the graph. The variation of σ^0 at X band shows more irregularities. The highest backscatter is found for the smallest radius represented (r_c=0.1 cm) and shows a sharp drop from r_c=0.1 cm to r_c=0.4 cm. For $r_c > 0.4$ cm, the backscatter at X-band is comparable to C-band. The important feature of the variation of σ^0 at C-band is that it is the most significant of the 4 bands for radii ranging for 0.1 to 0.4 cm. Most crops like wheat are composed of stalks whose radius is contained in this range. From this point of view, C-band is the frequency range for which the radar is sensitive to a significant fraction of the total biomass

of the crop. L and P bands are more suited for forestry applications, as these last two frequency ranges are sensitive to cylinder radii corresponding to tree branches. This result is confirmed by a similar independent study [55], using another radiative transfer model. The conclusion here is that C band SARs are adapted to the study of agricultural crops.

The variation of σ^0(HV) (Figure 3.1(c)) shows again the different radius ranges at which the backscatter for each band is most significant, but the backscatter intensities are much smaller. For that reason, the use of cross-polarisation for radar observations of crops is not particularly adapted.

3.2.2 Influence of stalk inclination

In order to study the influence of the orientation of the stalks as an independent parameter, the scattering volume is defined in RT2 to consist of cylinders of 5 different types (the maximum authorised by RT2). The radius of the 5 cylinders ranges from 0.1 cm to 0.5 cm, in increments of 0.1 cm. As shown above, it is the range of interest for the X and C bands so the analysis will focus on them. The number density of each of the 5 cylinder types is such that each type represents the same biomass. In other words, the number density is inversely proportional to the volume of each cylinder type. The incidence angle of the radar is set to 45° and the inclination angle α of the cylinders is the same for all 5 cylinder types and varied from 15° to 75°. Appendix A.1 gives the definition of α: it is the angle between the principal axis of the cylinders and the vertical.

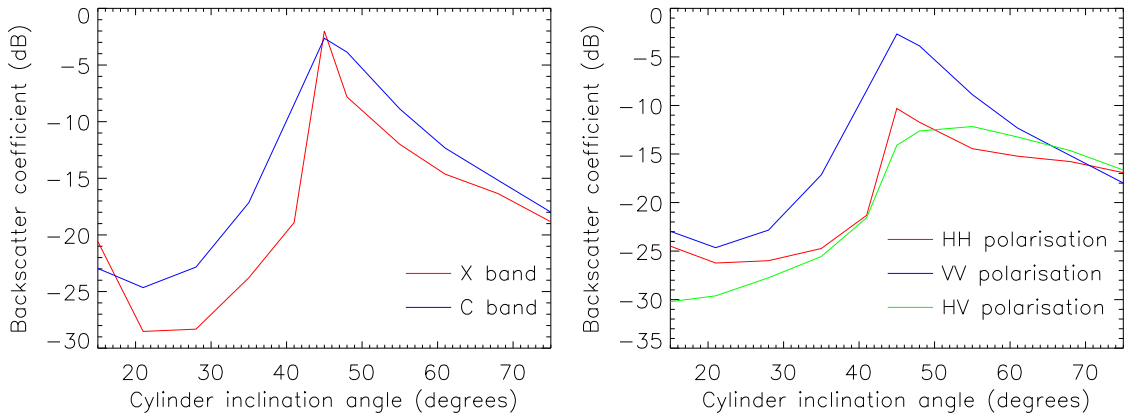

(a) VV polarisation, X and C bands

(b) C-Band, VV, HH, and HV polarisations

Figure 3.2: Variation of σ^0 with the stalk inclination angle α

Figure 3.2(a) shows that there is a strong dependence of the backscatter on the stalk inclination both at X and C bands. For $\alpha < 30°$, σ^0 is low because the radar wave is scattered mostly in the lower half space below the radar antenna. The peak backscatter intensity is clearly marked at $\alpha = 45°$, which corresponds to the radar incidence angle. σ^0 decreases for $\alpha > 45°$ as the specular reflection direction is above the radar antenna. Both the X and C bands show this behaviour, with a

higher backscatter intensity at C-band, due to the fact that σ^0_{C-band} is more sensitive to the range of cylinder radii used for the simulation, as explained in the previous section. The dependence of σ^0 with α is also a feature specific to VV polarisation, as it can be seen in Figure 3.2(b): σ^0_{HH} does not show the significant peak of σ^0_{VV} at $\alpha = 45°$. This is related to the fact that, for an horizontally polarised incoming wave, the electric field is orthogonal to the stalks whereas, for vertical polarisation, there is always a component of the electric field aligned with the stalks. This vertical component provides some coupling with the cylinders [18], which infers a higher sensitivity to the inclination of the scatterers.

From the results above, the importance of the structure of the plant and the radar polarisation is highlighted. Crops with a pronounced vertical structure like wheat or corn are expected to return a backscatter intensity higher at VV polarisation than at HH as there is a stronger interaction with a vertically polarised radar wave. The comparison of the VV and HH returns could in principle be used to differentiate crops with different structures. In addition to this, and relating these conclusions to the main concern of the research, the coherence should also be affected differently depending if it is derived from HH or VV SAR data.

3.2.3 Conclusions on the analysis

The two sets of results presented above indicate that a C-Band SAR with multiple polarisations is most suited to the remote sensing of crops. The C-band frequencies provide the highest backscatter return for stalk sizes typical of agricultural plants, and the horizontal and vertical polarisations govern different scattering mechanisms in vertically structured crops.

The vegetation orientation having a direct impact on the backscatter intensity, some information about how this orientation is affected by the wind seems relevant to the development of accurate backscattering models. Although it is beyond the scope of this research to use the measured crop motion information for that purpose, the relevance and potential use of the motion data is acknowledged here.

3.3 RT2 simulations for a wheat field: comparison with observations

In this section RT2 is used to model the backscatter intensity from a wheat field, at C-band ($\lambda = 5.66cm$), for incidence angles ranging from $\theta = 10°$ to $\theta = 70°$. The wheat field and the surface are modelled using the data published in [1], which is doubly interesting because it also gives radar observations from the wheat field, so the backscatter coefficient modelled here is compared to these radar data.

3.3.1 RT2 input parameters

A complete list of the parameters used for the RT2 simulation is given in Appendix A.4. The wheat is modelled as a single vegetation layer containing stalks and leaves. There are no wheat heads at the time of observation. The stalks are vertically

oriented, with a Gaussian distribution of mean 0° and standard deviation 10°. The leaves are set to be uniformly distributed in a $[0°, 90°]$ range. The size of the stalks and leaves and the leaf number density are obtained from [1]. In addition to the backscatter intensity, RT2 outputs the Mueller matrix from which the contributions to the total backscatter from the different scattering mechanisms is calculated.

3.3.2 Total backscatter

Figure 3.3 shows the expected total backscatter intensity from the modelled wheat, for HH and VV polarisations. The measured values of σ^0 given in [1] are plotted on the same graph for comparison.

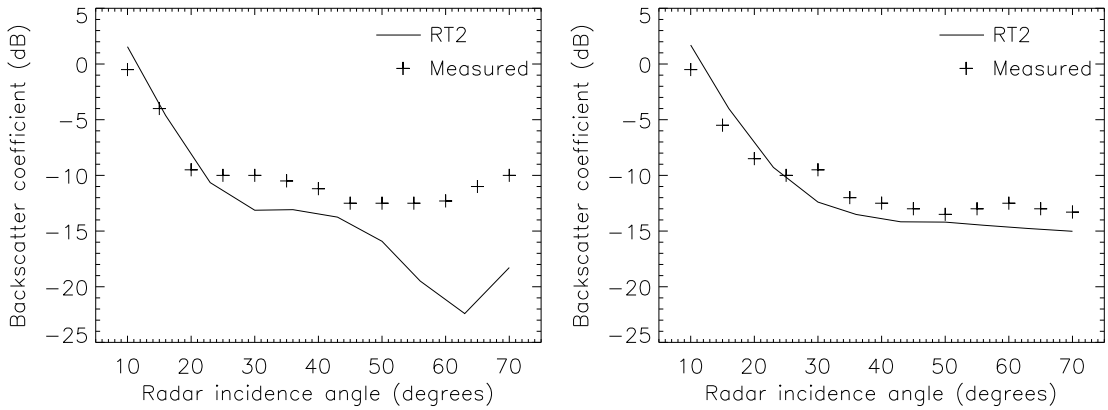

(a) VV polarisation

(b) HH polarisation

Figure 3.3: Total backscatter at C-band from a wheat field: RT2 estimates as a function of the radar incidence angle, and radar backscatter measurements obtained in [1]

Good agreement is obtained for the HH polarisation, with a root mean square error of about 2 dB. σ^0 decreases as the radar incidence angle θ increases due to the fact that, for θ close to 0°, the radar antenna is closer to the direction of specular reflection. The possible causes of difference between the model and the true data are either measurement errors in the radar data, or a wrong representation of the vegetation layer in RT2.

The model output for VV polarisation does not follow the measurements as closely, especially for $\theta > 50°$. A possible explanation for the high error in the model prediction may be that RT2 takes into account the Brewster effect which is not found in the backscatter measurements. From the theory of plane-wave transmission it can be shown that, for a vertically polarised wave incident from a medium 1 to a medium 2, there is an angle θ_B at which total transmission (i.e. no reflection) occurs. θ_B is called the Brewster angle. The total transmission emerging from the theory of plane wave transmission concerns only the vertically polarised waves [17], and its consequence is to reduce the radar backscatter. In the case of Figure 3.3(a), it is assumed that σ^0_{VV} is attenuated by the Brewster effect in the RT2 model, but this effect is not physically present in the radar observations.

3.3.3 Contributions from the different backscatter processes

Figure 3.4 shows the estimated contributions to σ^0 from the surface, the direct scattering from the vegetation, and the double bounce surface-vegetation backscatter.

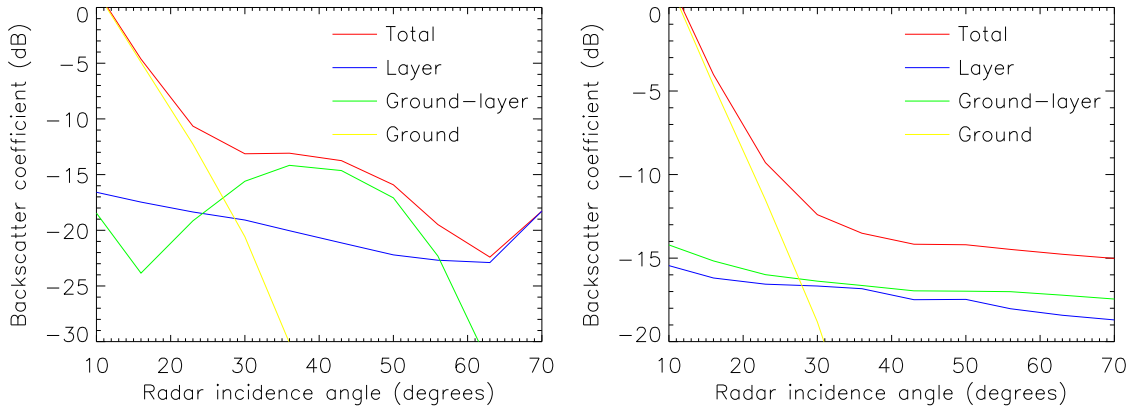

(a) VV polarisation

(b) HH polarisation

Figure 3.4: Contributions to the total backscatter from the different backscatter processes as a function of the radar incidence angle, for a wheat field

At low incidence angles ($\theta < 25°$), the main backscattering contribution is that of the surface. It should be noted in passing that the radar incidence angle for ERS is about 23°. Consequently it should be expected that an ERS image of the wheat field dealt with here would yield σ^0 values of about -6, -7 dB with a dominant backscattering contribution from the surface. As θ increases, the contributions of the vegetation layer becomes more significant. For VV polarisation, the contribution of the double bounce vegetation-surface peaks at about 45°. This specific interaction of the vertically polarised incoming wave with the wheat stalk was already mentioned in section 3.2. $\theta = 45°$ is the incidence angle required for the double bounce between a vertical structure (the stalk) and a horizontal surface (the ground) to be received back at the radar antenna. The peak is broad in Figure 3.4(a) because the inclination of the stalks was set in RT2 to have a Gaussian distribution with a 10° standard deviation.

The contribution of the direct scattering from the vegetation layer shows little variation, both for VV and HH polarisations. This contribution is that of the wheat leaves which are uniformly oriented in the scattering volume in all inclination angles, and therefore do not show any dependence to the radar incidence angle. The increase of σ^0_{VV} for $\theta > 65°$ is probably due to direct scattering from the wheat stalks.

3.3.4 Conclusion on the modelled backscatter intensity from wheat

In the previous example the RT2 model has shown some of its strengths and weaknesses. The strength of the model certainly lies in its capacity to estimate the contributions to the total σ^0 from the different scattering mechanisms. The fact

that the model predicts a different variation of these contributions for VV and HH polarisation and that these differences can be explained physically is a good indicator that the model outputs can be trusted in that respect, at least qualitatively. However RT2 has also shown that it predicts phenomena such as the Brewster effect which are not found in real data. This is difficult to avoid since all models imply simplifications of the reality, but it certainly means that the RT2 outputs should be treated with care at high incidence angles.

Bearing in mind the different conclusions and limitations about RT2 stated in the analyses above, the model can be used for the modelling of the coherence, as explained in the next section.

3.4 Statistical modelling of the coherence

The coherence model was originally presented in [47]. This section describes its basis and discusses its assumptions. Further sections in this chapter will then move on to present some outputs of the model, and will show how it is used to derive some requirements on the motion measurements.

3.4.1 Theoretical foundation of the model

The model assumes that the scattering volume describing the vegetation is composed of scatterers with different responses to the weather. While the soil can be expected to have constant properties with respect to wind (but not rain), the leaves, stalks, etc, of a crop usually have a specific response to weather conditions. The idea behind the coherence model is to separate the several scattering contributions, estimate their dependence to weather, and add them coherently to simulate the electric field received at the radar antenna.

The model assumes that the electric field returned from the target can be divided into a component which comprises the static part of the scene (V_s) and a component which is weather dependent (dynamic component V_d). In fact there can be as many weather dependent components as required, if more than one dependence is to be accounted for. Figure 3.5 is a phasor diagram representing the electric field components and introducing the variables.

Static component V_s

$\mathbf{V_s} = \mathrm{a}\exp(\mathrm{j}\varphi_\mathrm{s})$ is the static component of the electric field. It is assumed that it contains all the speckle properties of the resulting electric field, so its amplitude and phase have the following properties (see section 2.2.3):

- φ_s is uniformly distributed in the range [0,2π]
- a follows a Rayleigh probability distribution:

$$P(a) = \frac{2a}{\sigma_a}\exp\left(-\frac{a}{\sigma_a}\right) \tag{3.1}$$

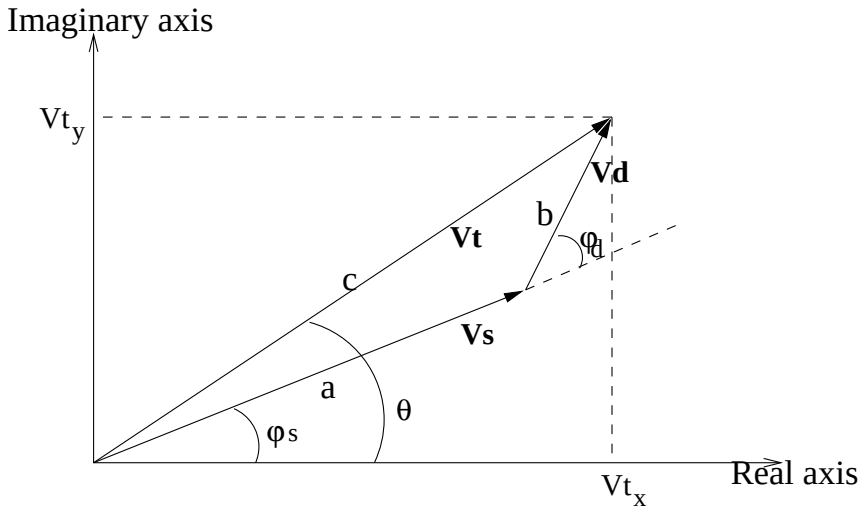

Figure 3.5: Phasor diagram representing the total electric field V_t and its static and weather dependent component (V_s and V_d respectively)

Dynamic component V_d

The dynamic component $\mathbf{V_d} = \mathrm{b}\exp\left[\mathrm{j}\left(\varphi_\mathrm{s} + \varphi_\mathrm{d}\right)\right]$ is specified by a probability distribution for the amplitude b and the added phase φ_d. The position of a scatterer in the scattering volume determines the phase of the signal backscattered from this scatterer. As it moves in the wind, the signal received at the radar antenna has a different phase for each of the scatterer's positions along the radar look direction. The phase of the dynamic component is therefore related to the motion of the scatterers subject to wind forcing.

The position of a moving scatterer in the vegetation volume being unknown at the time of the radar passes, the model assumes that the phase φ_d is a random variable whose distribution is related to the displacement of the scatterer in the look direction of the radar. This is where it is necessary to use motion measurements from crops. As a first approximation, the probability distribution of φ_d can be assumed to be Gaussian. The standard deviation of the distribution is directly related to the amplitude of the motion and therefore to the wind conditions.

The amplitude of the dynamic component is to be determined relatively to the amplitude of the static component. For that purpose it is necessary to estimate the contributions to the total backscatter from the different scattering mechanisms. The surface scattering contribution will feed into the static component of the model, whereas the contribution from the vegetation layer will be related to the dynamic part of the total electric field.

Computation of the resultant total electric field

The resultant electric field is computed as a phasor addition of the static and dynamic components. The model here is described with a single weather dependence, but another one or more can be added through successive phasor additions.

The model simulates two sets of N values for the total electric field, each set representing N independent pixels from a homogeneous target as they would be

recorded in one pass of the SAR antenna. Each of these N values is the complex addition of a fixed static component with a variable dynamic component having a random phase φ_d. Each value of φ_d is a random variable but the N values generated are such that they follow the statistical distribution defined for φ_d. With the two sets of N pixels, the resulting coherence can be calculated, according to the definition of Equation (2.24).

3.4.2 Practical implementation

Amplitude of the complex components

Section 3.3 showed how RT2 can be used to estimate the relative contributions to the total σ^0. The scattering contributions are surface scattering, direct scattering from the vegetation layer, the double scattering between the surface and the vegetation.

To illustrate how the dynamic components are specified, it is useful to take the example of the wheat field described in section 3.3. The double scattering was related to a double bounce of the radar wave on the stalks and the ground. For that reason the double scattering contribution is used here to model a first dynamic component corresponding to the motion of stalks. The direct backscatter from the vegetation layer is attributed to the leaves mainly, and consequently a second dynamic component is introduced to account for their specific motion.

The choice of the number of dynamic components therefore depends on the vegetation layer described and on the scattering mechanisms identified. Each dynamic component is related to a particular scattering mechanism, and RT2 provides an estimate of their amplitude, relative to each other and to the amplitude of the static component. In the case of a short time between the two radar passes (e.g. up to a few days), the same RT2 estimates can be used to determine the amplitude of the components for the two sets of simulated pixels. If significant changes have occurred during the two passes (e.g. phenological change due to growth, man-made changes), then separate RT2 simulations are required for the two crop states, and the two sets of N pixels are generated with different relative amplitude for the components of the total electric field. It should also be noted that RT2 is used here not so much for its capability to estimate the absolute values of the different contributions but rather values relative to each other. The relative amplitude of the static and dynamic components is of importance in the coherence model.

More flexibility is added to the coherence model by allowing the possibility for the amplitude of the dynamic components to be specified as a random variable defined by a probability function. By default, the probability function is assumed to be Gaussian. The mean of the probability function is the estimate provided by RT2, and its standard deviation is chosen to represent the variability of the backscatter intensity related to weather conditions. Several cases can be considered here:

- In the case of a short time between the 2 radar passes, and in the absence of rain between these passes, the dielectric properties of leaves and stalks are assumed to be constant and consequently the standard deviation on the amplitude of the dynamic components is set to 0.

- If rain occurred before one of the passes or even the 2 passes, then the stan-

dard deviation on the dynamic components can be set to a non-zero value to account for the possible uneven drying of the crop, which can result in different backscattering behaviour between adjacent pixels. This effect has not been studied in the research, but it is worth noting that the coherence model can include it.

- Any effect which can result in a variability of the backscatter from the vegetation can be accounted for as a resulting standard deviation on the amplitude of the dynamic components (man-made changes, uneven crop health due to micrometeorological conditions or local disease, etc...).

In the remainder of this report, the amplitude of the component is set to a constant value, so only the first case of the list above is considered. However, weather effects on the backscatter intensity can in principle be included for the simulation of coherence values.

The static component of the total electric field, a, is assumed to originate only from the surface scattering contribution. This assumption is discussed later in the chapter. The amplitude of the static component requires the definition of the standard deviation σ_a, which defines the Rayleigh distribution. For such distributions the standard deviation and the mean are related by [21]:

$$\mu_a = \frac{\sqrt{\pi\sigma_a}}{2} \tag{3.2}$$

The mean μ_a is taken here as the surface scattering contribution provided by RT2. So σ_a is calculated from Equation (3.2), and a value of a is generated from the Rayleigh distribution of Equation (3.1).

Generation of the phase probability distribution of the dynamic components

It is assumed here that the displacements of a particular scatterer in its natural environment have been measured, and are in the form of coordinates (x, y, z) in a fixed reference system. In the absence of data from field measurements, the model can also be run with *a priori* phase distributions such as a Gaussian.

An important assumption made at this stage is that each weather dependent component of the electric field is represented by a single scatterer whose motion characterises the motion of all scatterers of the same type in the radar ground resolution cell. This assumption is discussed later, in section 3.4.3. The problem to solve here is, given a radar look direction and the position of this equivalent scatterer in a coordinate system, to determine its displacement along the radar look direction. From a time series of its positions, the corresponding displacements in slant range can then be calculated and translated into a phase shift. The phase values obtained from all slant range displacements are used to generate a histogram which, after normalisation, is the probability function defining the random phase φ_d of the dynamic component of the electric field.

Figure 3.6 shows the geometry and introduces the necessary variables. The origin of the reference system is taken at the mean position of the scatterer. The system of axes is defined so that (X,Y) is a horizontal plane and the Z axis points to the

vertical upwards. The direction of the X axis is chosen so it can be conveniently related to any physical feature. The three-dimensional position of the scatterer at a given time, relative to its mean position, is defined by its coordinates (x, y, z). The radar look direction is defined by its azimuth α and its view angle β (β is complementary to the radar incidence angle). The look direction of the radar is defined by a straight line (D). $\mathbf{u_D}$ is a unit vector of (D). P' is the projection of P on (D). In the following equations, vectors are noted in bold and scalars in plain text.

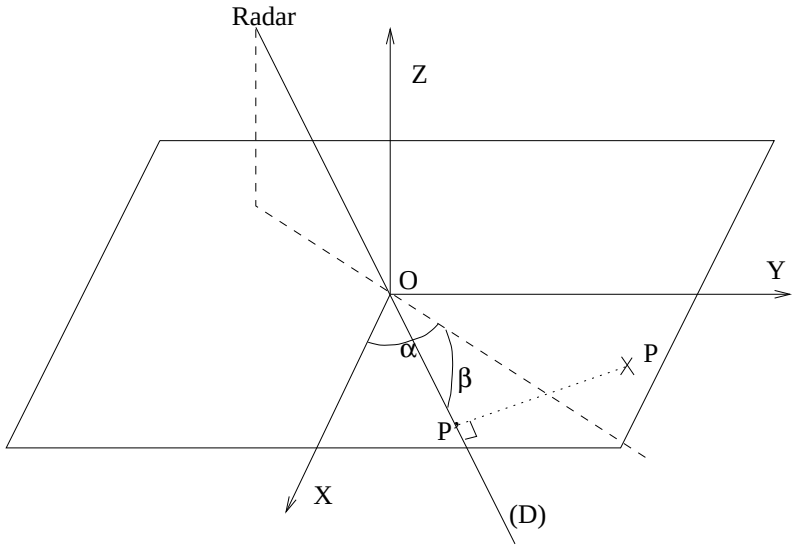

Figure 3.6: Geometry and variables for the calculation of the slant range displacement of a scatterer

Since P' $\in$ (D), $\mathbf{OP'} = k\mathbf{u_D}$, and k is the scalar value defining the slant range displacement of P along the radar look direction. The coordinates $(x_{u_D}, y_{u_D}, z_{u_D})$ of the unit vector $\mathbf{u_D}$ are:

$$\begin{aligned} x_{u_D} &= \cos\alpha\cos\beta \\ y_{u_D} &= \sin\alpha\cos\beta \\ z_{u_D} &= \sin\beta \end{aligned} \tag{3.3}$$

P' being the projection of P on (D), the scalar product of $\mathbf{OP'}$ and $\mathbf{PP'}$ is zero:

$$\mathbf{OP'}.\mathbf{PP'} = 0 \tag{3.4}$$

Using the notation introduced above, Equation (3.4) can be written:

$$k\mathbf{u_D}\,(k\mathbf{u_D} - \mathbf{OP}) = 0 \tag{3.5}$$

After development it becomes:

$$k\,[k - (x\cos\alpha\cos\beta + y\sin\alpha\cos\beta + z\sin\beta)] = 0 \tag{3.6}$$

So the slant range displacement of P is:

$$k(x, y, z) = x\cos\alpha\cos\beta + y\sin\alpha\cos\beta + z\sin\beta \tag{3.7}$$

$k(x, y, z)$ is calculated for every position of P, and the slant range probability distribution is the normalised histogram of the values of k. With a randomly selected slant range value r from the probability distribution, the associated phase is:

$$\varphi_d = \frac{4\pi}{\lambda} r \tag{3.8}$$

where λ is the radar wavelength. The values of r therefore define values of φ_d whose normalised distribution defines the probability density function of the phase of the electric field dynamic component. The probability density function of φ_d is used in the model to generate the complex pixel values from which the coherence is calculated.

Computation of the coherence

There are N pixels simulated for each of the two radar passes. N is set to a high value (e.g. 1000) so the coherence bias at low values is negligible (see the discussion on coherence statistics in section 2.2.4). For each pixel, the electric field V_{t_i} (i=1,2: index of the radar pass) is computed by following the steps below:

- The RT2 estimates of the scattering contributions are used to calculate the amplitudes of the static (a_i) and dynamic components (b_{ij}, j: index of the dynamic component). The RT2 outputs are proportional to the power received at the antenna from the several scattering mechanisms, and are expressed in dB. Therefore, for a scattering contribution estimated by a value σ_j^0(dB), the amplitude b_{ij} of the dynamic component associated to it is:

$$b_{ij} = \sqrt{\exp\left(\frac{\ln 10}{10}\sigma_j^0(dB)\right)} \tag{3.9}$$

- The phase of the static component φ_{s_i} is taken from a random number generator following a uniform distribution. All pixels of one set use the same value of φ_{s_i}.

- The phase of the dynamic components $\varphi_{d_{ij}}$ is calculated from the random selection of a slant range value following the distributions derived from the motion observations (see explanations above). The random selection of a slant range r from the probability distribution is performed numerically, using an algorithm based on the rejection method presented in [56].

- From these numerical inputs, the total electric field for a single pixel is:

$$V_{t_i} = V_{t_{i_x}} + jV_{t_{i_y}} \tag{3.10}$$

with:

$$V_{t_{i_x}} = a_i \cos\varphi_{s_i} + \sum_j b_{ij} \cos\left(\varphi_{s_i} + \varphi_{d_{ij}}\right) \tag{3.11}$$

$$V_{t_{i_y}} = a_i \sin\varphi_{s_i} + \sum_j b_{ij} \sin\left(\varphi_{s_i} + \varphi_{d_{ij}}\right) \tag{3.12}$$

Each pixel from the same set, representing a data point from a single radar pass, is generated with a common value of the static component. After the generation of the two sets of N complex values, the coherence is calculated from Equation (2.24).

Since the computation requires the generation of random numbers from different probability distributions, it is worth making here a few comments on how these numbers are generated. IDL is the language used for the computation described above. It has a random number generator based on the definition of an initial seed whose value is determined by the system clock. In most applications this is sufficient but in the case presented here, the random numbers are needed at a rate faster than the refresh rate of the seed. In other words, some random numbers, which are required to be independent for the calculation, originate from the same initial seed, before it has been changed by the system clock (the initial seed in IDL is refreshed every second). To overcome this problem, the initial seeds are not chosen from the system clock but from an initial seed list, itself generated at the beginning of the program by the IDL random number generator. The seed list is updated when all its values have been used in the computation. Operating in this way allows to have a set of numbers whose random nature is limited only by the IDL random generation algorithm.

3.4.3 Discussion of the model

It is important at this stage to comment on the coherence model presented above, and on its relation to the true backscatter mechanisms in a vegetation layer. The static component of the model contains all the speckle properties of the pixel, i.e. the speckle introduced by the soil and also by the vegetation. The dynamic components do not account for the speckle but are described as extra terms in the total backscatter electric field. In real backscatter mechanisms, these extra terms are not physically added to a static component because the contributions of the vegetation also generate speckle in the resultant image. However, artificially separating the total electric field into a static part which accounts for the speckle, and a dynamic part which does not, allows to isolate the dependence to weather conditions which are of prime interest here.

Contribution to the static component from the vegetation

The limitation with the model approach is that it is not physically possible to know exactly which part of the signal is viewed as static (i.e. unchanged between the two passes) by the radar, and which part is viewed as dynamic, i.e. changed between the two passes of the SAR. So these parts have to be estimated. A starting point consists of using what is known about the backscatter estimated from RT2. The contribution of the soil is assumed to be always 100% static. The contributions of the crop elements is (1-κ)*100% static, where κ is an unknown factor between 0 and 1. The parameter κ is dependent on the wavelength. Part of the crop will be viewed as static by the radar if:

- a corresponding scattering element does not move between the two radar passes,

- a scattering element in the first pass is replaced in the same geometric configuration by another one in the second pass,

- a scattering element moves in the slant range direction by an amount corresponding to a multiple of the phase cycle (i.e. by a multiple of the wavelength).

Intuitively, these cases have a small probability to be found: there will always be a difference in position/geometry of the scatterers and replacement of one element by another in the same configuration, at the time of the second radar pass, is virtually impossible. So in practice, the value of κ is probably very small. It will be taken as 0, which means that the vegetation medium will be considered as a totally dynamic medium. In fact, if the scatterers in the vegetation do not move, it will be reflected in the slant range distribution derived from the observations: the distribution will show a very narrow peak corresponding to a single position of the scatterer. The case of a static vegetation is therefore also included as a possibility in the model. The dynamic parts of the backscatter being taken as the entire contribution from the vegetation, their intensity is given by RT2 and fixed (except for possible changes in moisture or growth).

Concept of equivalent scatterer

Another central point in the coherence model is that is assumes that all scatterers which are grouped in a single weather dependence move as a single equivalent scatterer. The validity of this assumption depends on the scale at which the problem is considered. Obviously, at a field scale, scatterers of the same type do not all move in phase and the concept of equivalent scatterer does not hold for them. At the other extreme, at a reduced scale (typically, tens of centimeters), the crop plants have a motion which is much more correlated, sometimes even exactly in phase because of the mechanical interactions between plants though direct contact. In this case the concept of an equivalent scatterer is valid.

Consequently the validity of the equivalent scatterer assumption depends on the resolution of the SAR. For very fine resolutions, a single dynamic component accounts for the motion of all scatterers in the ground resolution cell. A fine resolution for this assumption to hold is less than a metre, and is currently potentially achievable only from airborne SARs. For lower resolutions (spaceborne SARs), all scatterers in the ground resolution cell cannot be represented by a single synchronised motion. However, it is possible to introduce in the model as many dynamic components as there are "packets" of coherent motion of the crop in the ground resolution cell.

So it is a requirement of the crop motion measurements to be made to provide some quantitative information about the spatial correlation of the motion. For that purpose the motion of the crop should be measured on different plants and the cross-correlation between the individual displacement of the plants can give a quantitative idea of the spatial correlation of the motion, which in turn can help to define the scale at which the scatterers can be said to move coherently.

The concept of an equivalent scatterer is central to the model. It means that the scattering from a ground resolution cell is summarised by a single scatterer whose

properties are such that it includes the standard speckle properties of a radar image and nevertheless takes into account the motion of crops as a phenomenon separate from the speckle effect. In reality the complex backscatter from the two radar passes is obtained from two different speckle patterns but cannot be artificially divided into a purely speckle part which is static and a purely non-speckle part which is dynamic. What the model says is that these patterns are generated with two surface configurations nearly identical except for a change in the position of the crop elements due to wind-induced sway. So it is a translation of the true physical mechanisms into workable terms which can take into account the effect of weather dependences such as wind.

It is clear that such a modelling approach does not relate directly to the true backscatter mechanisms which occur in a vegetation volume. Only a rigorous coherent backscatter model does account for these true scattering processes. However, the development of such a model requires a dedicated research, and solid experience in the domain of backscatter modelling. The statistical estimator described here is a simplification of the backscatter processes, but it will allow to show how the wheat motion measurements can be integrated into it. The preliminary tests of the model presented in the next section show that its outputs are useful to identify the key elements influencing the coherence.

3.5 Preliminary tests of the coherence model

This section shows some outputs of the coherence model. First, it is interesting to test the model in an artificial case not related to crops in order to check that it outputs expected results. Then the model is tested on wheat. The idea behind these preliminary tests is the same as in section 3.1.2, when the backscatter intensity was the main focus of attention. The aim is to determine the important parameters which influence the coherence.

3.5.1 Phase spread dependence

The coherence model is used here with a single dynamic component. The amplitude a of the static component is varied from 0 to 1 and the amplitude of the dynamic component is $1-a$. The phase of the dynamic component is set to follow a Gaussian distribution, with a mean equal to its standard deviation σ_{φ_d} (also called 'phase spread' in the following discussion) and varied from 0° to 180°. Figure 3.7 shows the results of the simulation.

For a given value of a, there is a decrease of the coherence (referred to as γ in the discussion below) with the phase spread, from 1 (σ_{φ_d}=0: no motion of the scatterers) to an asymptotic value which depends on the value of a. The asymptotic value is reached for $\sigma_{\varphi_d} \approx 110°$ and its value decreases with decreasing contribution from the static component of the model. For $a = 1$, the scene is entirely static and consequently the coherence remains equal to 1. When the scene is totally dynamic ($a = 0$), γ decreases to a non-zero asymptotic value. This is due to the fact that the calculation of the coherence from Equation (2.24), in the case of a totally dynamic scene, is equivalent to a random walk is the complex plane, and the magnitude of

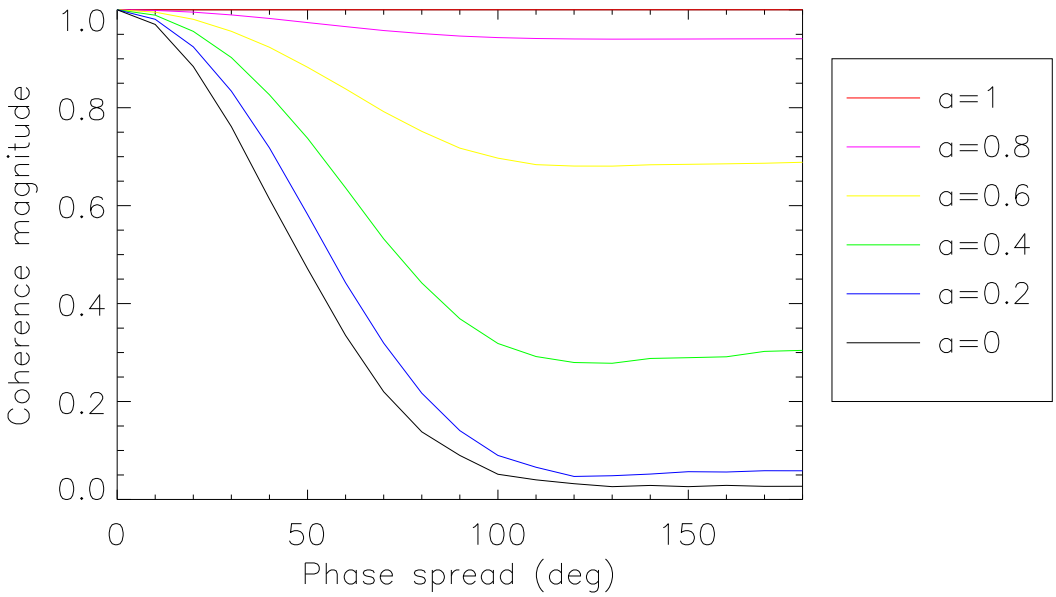

Figure 3.7: Coherence variation with the phase spread of the dynamic component, plotted for different values of the static contribution a

γ in this case tends to $1/\sqrt{N}$ [22], where N is the number of pixels used in the simulation. For the simulation here, N=1000, so the expected asymptotic value is about 0.03, which is the value observed in Figure 3.7 for $a = 0$.

For the intermediate cases ($0 < a < 1$), the variation of γ calls for a few comments, since it represents more closely the case of real vegetation. If the scatterers in the vegetation volume move by an amount superior to what is required to induce a phase spread of about 110°, then the coherence reaches an asymptotic value which is an indicator of the ratio between the static and dynamic components. A given motion amplitude in slant range translates into a higher phase spread at shorter wavelengths, and therefore the asymptotic value will be reached for smaller displacements at shorter wavelengths. In addition to this, the coherence decreases rapidly for intermediate phase spreads ($20° < \sigma_{\varphi_d} < 80°$). At these intermediate values, an uncertainty on the determination of the value of σ_{φ_d} from the motion measurement translates into an uncertainty of the coherence estimates from the model. Therefore, the accuracy required on the coherence estimates from the model will drive the accuracy in the determination of σ_{φ_d}, which in turn will impose a precision requirement on the motion measurements. This aspect will be detailed in the next section, but it is mentioned here to emphasise the fact that the preliminary test presented here is directly relevant to the objectives of the research.

In practice, the coherence derived from SAR data above vegetation is typically in the range [0.3,0.7], depending on the type of vegetation. The model shows that these values can be reached in two ways: either by a scene where the vegetation is responsible for most of the backscatter and has a moderate movement which induces a phase spread inferior to about 110°, or by a scene where the surface scattering plays a major role, with a vegetation motion high enough to reach the asymptotic value for γ.

To illustrate this point, it is interesting to take a numerical example. In the

case of ERS-1/2, the wavelength λ is 5.66 cm and the incidence angle is $\theta = 23°$. A variation $\delta\varphi_d = 110°$ is induced by a scatterer motion in the slant range direction $\delta r = (\lambda/4\pi)\delta\varphi_d = 0.86cm$. This corresponds to an horizontal displacement $\delta h = \delta r/\sin\theta = 2.21cm$. The simulation above has assumed a Gaussian distribution, which is symmetrical about its mean value, so the total amplitude of the horizontal motion above which the asymptotic value of γ is reached is $2\delta r = 4.42cm$. Intuitively, it is likely that crops move by a greater amount in windy conditions and the coherence values observed with ERS data represent the asymptotic value of γ. The coherence observed from ERS SAR data from crops being in the intermediate region [0.3,0.7], the natural conclusion here is to assume that the contribution to the total backscatter from the surface is fairly high. Indeed this result was noted in section 3.3, Figure 3.4, where the RT2 simulation of a wheat field showed that a significant part of the backscatter originates from the surface at incidence angle of about 20°.

The example above is interesting in two respects. First it shows that the outputs of the coherence model make good sense when compared qualitatively with the SAR coherence data. For that reason it can be used with confidence to interpret some of the features related to the coherence behaviour above crops. Secondly, the example above showed how issues concerning the radar specifications (wavelength, incidence angle) relate to the coherence. The model provides a link for the quantitative analysis of the interactions between the two.

3.5.2 Wheat simulation

The coherence model is run here with the outputs of RT2 presented in section 3.3. The analysis shows the variation of coherence with the incidence angle θ for a constant radar wavelength $\lambda = 5.66$ cm.

Input parameters

The contributions showed in Figure 3.4 are used in the model to define the relative amplitude of the static and dynamic components of the total electric field. Two dynamic components are introduced. The first dynamic component is related to the motion of the wheat stalks. The amplitude of the component is taken as the vegetation-surface (double-bounce) contribution given by RT2 (referring to the discussion given in section 3.3 on that point). The phase distribution function is taken as Gaussian, since no other motion information is available at this stage. The standard deviation of the distribution (the phase spread $\sigma_{\varphi_{d1}}$) varies with slant range spread dr: $\sigma_{\varphi_{d1}} = (4\pi/\lambda)dr$. Slant range spreads dr ranging from 0 to 1 cm were tested in order to assess the influence of the motion amplitude on the coherence. The second dynamic component of the model reflects the motion of the leaves, which are assumed to contribute to the direct scattering from the vegetation layer (see section 3.3). The phase φ_{d2} has a Gaussian distribution whose standard deviation is set to be identical to the standard deviation of the first dynamic component. This assumption means that the motion of the leaves is set to have the same amplitude as that of the stalks. It is very difficult to verify this assumption without field observations. Since the leaves are physically connected to the stalks, this assumption

is reasonable, although it does not take into account the relative motion between these two components of a wheat plant.

Model outputs

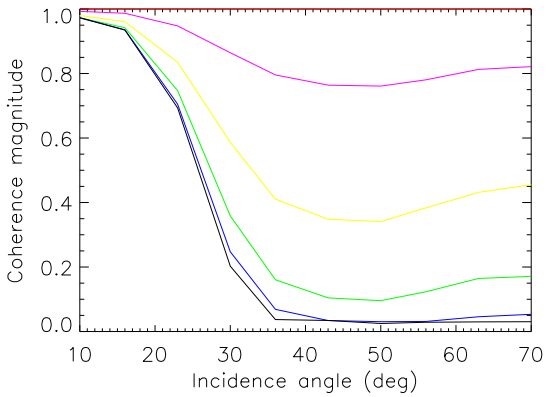

(a) VV polarisation

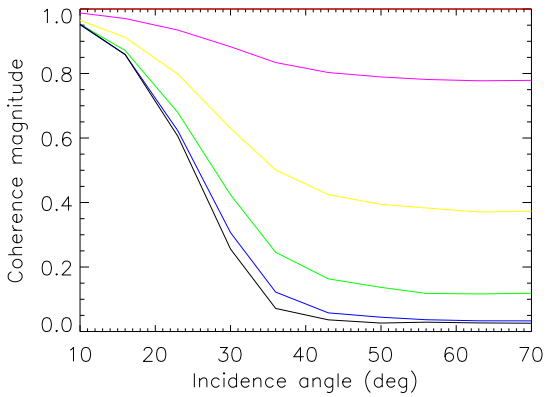

(b) HH polarisation

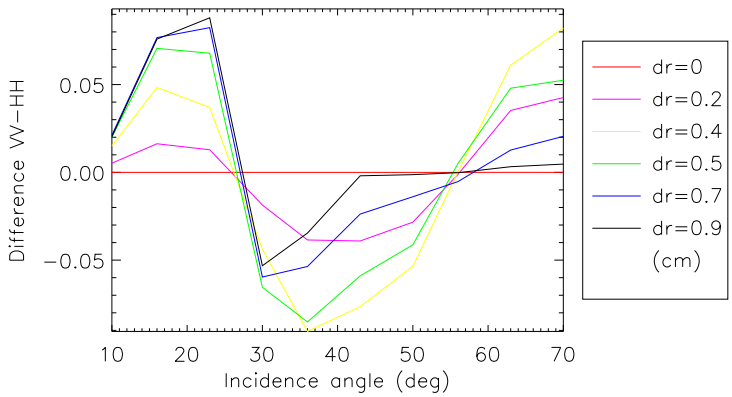

(c) Difference VV-HH

Figure 3.8: Variation of the estimated coherence with the radar incidence angle, plotted for 5 different slant range spreads dr, and from the RT2 outputs obtained in section 3.3 for VV and HH polarisations

Figure 3.8 shows the outputs of the model for HH and VV polarisations. The estimated coherence is plotted against the radar incidence angle for different values of the slant range spread characterising the motion of the wheat stalks and leaves. For a given slant range dr spread, the coherence decreases rapidly with the incidence angle for $\theta \in [10°, 30°]$. This feature is to link with the rapid decrease of the surface scattering contribution shown in Figure 3.4 for the same incidence angle range. For $\theta > 30°$ the surface contribution becomes negligible, so the static component of the coherence model also becomes negligible, and the total electric field is resulting from the addition of the two dynamic components. In this case the coherence remains

approximately constant at a level related to the amount of motion assumed in the vegetation.

The coherence given by the model for the ERS incidence angle ($\theta \approx 23°$) is in the range [0.5-0.7], which corresponds to the values obtained from ERS data above agricultural surface. Even with crude approximations about the vegetation motion, it seems that the model is able to predict the observed coherence level. Another point to note is the sensitivity of the coherence to the incidence angle around $\theta = 25°$. Radar incidence angles of about 25° seem appropriate to crop monitoring since different crops would in principle show a significantly different coherence sensitivity around this value. For higher incidence angles, the coherence levels observed from different crops would yield consistently low coherence values which would be of no use for classification or other monitoring purposes.

Figure 3.8(c) shows the difference between the coherence obtained from VV and HH polarisations. It was shown is section 3.3, Figure 3.4, that a vertically polarised incident wave is more coupled to vertically structured crops like wheat, so there should be a visible difference on the coherence from this physical effect. Figure 3.8(c) shows that there is a maximum positive difference between the VV and HH coherence at $\theta \approx 23°$. The rapid decrease of the coherence at such incidence angles explains that larger differences are found between the VV and HH polarisations. For $30° < \theta < 55°$, the difference between the VV and HH coherence is negative. This is to relate to the specific variation of the stalk-ground contribution at VV polarisation (see Figure 3.4(a)). At HH polarisation, the contributions from direct scattering and double scattering remains roughly constant and, more importantly, in the same ratio. At VV polarisation the double scattering contribution peaks at about 45°, so the dynamic component related to the stalk motion has a peaking contribution at this angle. At this peak contribution, there is additional decorrelation introduced in comparison to the HH polarisation, and consequently the VV coherence is lower. This explains the negative difference for $\theta \epsilon [30°, 50°]$ between the VV and HH coherence.

3.5.3 Conclusions on the preliminary tests of the model

The outputs of the coherence model have shown some of the key features which relate the crop parameters, the radar configuration, and the expected coherence. The sensitivity to the amplitude of the crop motion was highlighted, as well as the sensitivity to the radar wavelength and the incidence angle. At near vertical incidence angles, the contribution of surface scattering is dominant and there is little loss of coherence due to the motion of the scatterers. The very sensitive range of incidence angles, at which the coherence decreases rapidly, is situated around 25°, near the ERS value.

The examples above give a good overview of how the coherence model can be used to estimate the potential use of coherence as a parameter for crop monitoring. The study was focused on the C-Band since the study of section 3.2 has shown it is the most relevant frequency range for crop monitoring. At shorter wavelengths, it can be expected that the contribution to the total backscatter from the vegetation will be higher, inferring a higher loss of coherence for an equivalent crop motion.

In addition to this effect, the same motion amplitude translates into a higher phase spread at shorter wavelengths, adding to the decorrelation. The opposite conclusion applies to longer wavelengths.

The possible sources of inaccuracies in the model are:

- a wrong estimate of the phase standard deviations of the different dynamic components, and especially relative to each other,
- an inaccurate representation of the phase distribution by a Gaussian function,
- a possible error added by assuming a single "equivalent scatterer" in the ground resolution cell,
- inaccurate contribution estimates from RT2.

The next section will describe in more detail how the requirements to evaluate the first 3 points above translate into crop motion measurement requirements. The last point of the list is important since it was shown in the examples above that the estimation of the contributions from the different scattering processes is the major driver of the coherence levels given by the model. Accurate RT2 estimates require an accurate description of the crop phenotype, which can be difficult to obtain from the simple geometrical shapes available in RT2 and because of the lack of accurate data on crop characteristics.

3.6 Definition of measurement requirements

This section uses the description and preliminary tests of RT2 and the coherence model to define measurement requirements.

3.6.1 Meteorological data

Since the motion of the vegetation is directly responsible for the temporal decorrelation, it is important to have meteorological data. Two types of data are useful here. First it is necessary to know the wind velocity at the crop level in order to have a precise idea of the relation between crop motion and wind forcing. The wind at crop level is likely to be turbulent, so data should be recorded at a high sampling rate. The wind data sampling rate will be given and justified in Chapter 5. It is imposed by the accuracy limits of the equipment used.

In addition to wind data at canopy height, it is interesting to have some more general weather data, in order to make a quantitative estimate of the probability of certain weather conditions to be found at a given period in the growth season.

3.6.2 Crop motion data

The motion of crops under wind forcing is used to derive the probability distribution for the phase of the dynamic components of the coherence model. The distribution being derived from three-dimensional positions of the scatterers, the crop motion is

required in three dimensions too. There are two accuracy requirements on the motion measurements: requirement on a single plant, and requirement on neighbouring plants.

Measurement accuracy on a single plant

The standard deviation on the coherence estimates calculated from SAR data with Equation (2.24) is defined in [31] by:

$$\sigma_\gamma = \frac{1 - |\gamma|^2}{\sqrt{2N}} \tag{3.13}$$

where N is the number of pixels in the calculation window. Existing data from SAR observations shows that the coherence from agricultural crops is about 0.4 or higher. With a coherence calculation window containing 45 pixels (typically, a 3x15 window is used with ERS data), Equation (3.13) shows that σ_γ is inferior to about 0.1. This value is the accuracy requirement set for the coherence model. It needs to be translated into a position measurement accuracy.

Figure 3.7 shows that the most rapid decrease of the coherence with the phase spread $\delta\varphi_d$ occurs at around $\delta\varphi_d = 40°$ and the rate of the decrease (slope of the curve) is about $s = -0.12/10°$. Taking this worst case, if an accuracy of 0.1 is required for the coherence estimate, the phase spread should be retrieved from the measurements with an accuracy of $0.1/s \approx 8°$. A phase accuracy of 8° corresponds to $(1/45)\lambda$. Therefore the measurement accuracy of the system is related to the radar wavelength. Focusing on C-Band, a value of λ of 6 cm translates into a measurement accuracy of 1.3 mm in slant range. For crops having a motion mainly in a horizontal plane, it translate into an accuracy of $1.3/\sin\theta$, where θ is the radar incidence angle. At the ERS value of 23°, the measurement accuracy in a horizontal plane is about 3.3 mm. This is quite a stringent accuracy requirement, but it was derived from the highest variability of the coherence from Figure 3.7. It can be expected that, if an accuracy of 3.3 mm is achieved by the measurement system, the uncertainty on the coherence estimate from the model will be about 0.1.

Measurement on several plants

The requirement to check the "equivalent scatterer" assumption imposes requirements on the measurements of several plants. Ideally, motion measurements widely spaced (several metres) would be most suited to derive the number of packets of coherent motion within the ground resolution cell. However this is not practically achievable as it would require several measurement systems placed at different positions in the field, all synchronised with each other and with the wind data measurement system.

Alternatively, the motion of several plants can be measured in a smaller measurement volume, and cross-correlation functions between the measured motions will give information about the extent of the synchronised motion. The correlation functions will give a quantitative idea about the correlation distance, i.e the distance after which the motion of two plants is not correlated. For this correlation distance to be calculated accurately the motion of plants should be measured across

the whole space covered by the measurement volume. The size of this measurement volume is determined by the measurement system itself, and will be given in the next chapter.

3.6.3 Data synchronisation

The wind data at canopy level and the crop motion data need to be synchronised so they can be used in conjunction with each other. A precise synchronisation scheme is needed for that purpose. In addition to the time synchronisation of the data sets, there is a requirement to align the wind data reference system with the crop motion reference system.

3.6.4 Crop phenotypical state

The definition of the vegetation layer in RT2 requires a good knowledge of the crop phenotype. In fact, it is of prime importance since the previous sections have shown the importance of having an accurate estimate of the relative contributions to the total backscatter from the different scattering mechanisms. The parameters of importance include the density of the different scatterers, their gravimetric moisture, geometry, orientation, the surface roughness and correlation length. These parameters are needed at different stages of the crop growth. Even with a good knowledge of the crop phenotype, it was shown in [57] that making a good modelling with RT2 can be difficult.

Two aspects contribute to the decision that was made in the research to not measure the crop parameters *in situ*. First, the measurement of data of good quality is difficult and requires experience which was not available during the time of the research. It was decided not to collect data whose quality would have been questionable because of lack of experience and proper equipment. As RT2 requires a good definition of the crop phenotype, it is felt that the data which would have been collected locally would not have met the required standards of quality. The second reason which justifies the decision is that good crop data collection usually requires dedicated measurement campaigns which are time consuming. The research presented here covers a range of different topics and the time constraints imposed on the project did not allow the collection of crop phenotypic data, in addition to the time required to cover these other topics.

The need for accurate phenotypical data is nevertheless identified here as a requirement for the research. It is left as potential on-going work for future developments of the project. As an alternative solution to compensate for the lack of crop data, existing data sets can be used for RT2 simulations.

3.7 Conclusion

This chapter has presented some of the issues related to the relationship between the radar backscatter intensity, the coherence, and the vegetation. The few examples presented in the previous sections have shown the sensitive variables in this context. From the point of view of the backscatter intensity only, the RT2 outputs have

shown that a C-Band SAR is most suited for vegetation monitoring. In addition to this, it was shown how RT2 is a necessary tool for the coherence model since it estimates the independent contributions to the total backscatter. The coherence model uses a statistical approach which does not assume complete random motion of crop elements. It still relies on a simplification of the apparent complexity of crop motion, but it is a first step towards quantifying its effects.

The RT2 runs showed the influence of the size and orientation of the scattering elements. This influence suggests that the motion of these elements is a parameter to take into account, not only in the estimation of the coherence, but also in the modelling of the backscatter intensity. This is especially true if the motion is coherent in the ground resolution cell, and not totally decorrelated. Full decorrelation is commonly assumed to describe motion in a vegetation medium, which may not be the case. In fact the preliminary outputs of the coherence model tend to show that complete decorrelation of the scatterers motion would not explain the intermediate coherence levels observed from SAR data.

Backscatter models could benefit from more detailed crop motion information, and so could the coherence model. The main aim of this chapter is fulfilled: it was possible from the presentation of the two types of models to justify the need for *in situ* measurements. Not only the models could justify a need for these measurements, but they were also used to identify some more precise requirements. They concern the accuracy of the motion retrieval, the need for meteorological data and for several measurement points in the crop field.

The next chapters describe the measurements made for the research, and further use of the coherence model will be made in Chapter 7.